Istanbul Technical University
Electrical - Electronics Engineering Faculty

A READOUT METHOD FOR A FLUX QUBIT-RESONATOR SYSTEM IN THE ULTRASTRONG COUPLING REGIME

BSc. Thesis by
Ceren Burçak Dağ

Department: Electronics and Telecommunications Engineering
Programme: Electronics and Telecommunications Engineering

Supervisors:

Prof. Dr. Selçuk Paker
Istanbul Technical University

Dr. Pol Forn-Díaz
Institute for Quantum Computing

Assoc. Prof. Dr. Christopher Wilson
Institute for Quantum Computing

August 2014

Contents

List of Figures

Summary

Quantum Rabi Model is a system composed of a two-level system and a quantized oscillator. This model allows the exchange of an excitation between these two fundamental physical systems. The first attempt to solve for Quantum Rabi Model was made by Jaynes and Cummings, by applying the rotating wave approximation (RWA), which assumes that the coupling between the subsystems is much smaller than the frequency of the subsystems. Some theoretical analysis for the Quantum Rabi Model has been performed in the ultrastrong coupling regime which requires a comparable coupling strength with the frequency of the resonator and points to novel effects. It is not possible to discuss about the individual subsystems in the ultrastrong coupling regime and the whole system becomes a single integrated quantum system, which behaves quite distinct from the predictions of the Jaynes-Cummings model. In order to fully understand the physics behind the ultrastrong coupling regime, an intuitive mental picture is required, such as the photon wave packet dynamics in the parity state chains of the Quantum Rabi Model in Hilbert space. The ultrastrong coupling regime has also been introduced to flux qubit circuit-QED systems and the experiments performed so far have showed different characteristics of the regime. However, no one has achieved to apply a Quantum Nondemolition (QND) measurement to a circuit-QED system working in the ultrastrong coupling regime, yet. Such a measurement in general uses the dispersive regime by utilizing a readout resonator in a c-QED system to probe to a qubit without affecting the states of the qubit. The theoretical calculation of a QND measurement design for a flux qubit-resonator system in the ultrastrong coupling regime is the main motivation of this research. In order to achieve this goal, the Rabi Model with an additional weakly coupled resonator, the so-called readout resonator, is proposed to be added to the system. Different amounts of energy shifts are observed for the ground and first excited states of the system, which is a conclusion that shows the proposed QND mechanism is possible to construct for the experimental observation of the states of this quantum object. An analytic expression for the energy shifts is aimed to be derived for further research.

Chapter 1

Introduction

The study of light-matter interactions was always one of the integral parts of the physical curiosity throughout the history of science. As each part of physics was affected by the theory of quantum mechanics, the light-matter interactions were no exception. Planck needed to introduce the quanta of light, or photon, in order to solve the blackbody radiation problem in the beginning of the 20^{th} century, [2], which was the birth of the quantum mechanics. A full quantum mechanical treatment of light-matter interactions started with the quantization of the free electromagnetic field [3]. The idea of modelling the electromagnetic field as a collection of uncoupled harmonic oscillators for each mode existing in the field origins back to Jordan, [4]. However it was Dirac who combined the idea with the mechanics of matrices of Heisenberg to quantize the electromagnetic field. The representation of the field in terms of a collection of uncoupled harmonic oscillators reduced the problem to the quantization of the harmonic oscillator, which is one of the simplest and the most fundamental systems in physics.

A two-level system is another simple and basic element appearing in quantum mechanics. As its name implies, a two-level system spans 2×2 Hilbert space and the obvious example of a two-level system is the spin$-1/2$ particle [5, 6]. It is also possible to approximate a quantum object as two-level system if other states are farther away from particular two levels. Two-level systems are used as 'qubits' in quantum computing and information science [7].

The single mode qubit-photon system is in general a system composed of a two-level system and an oscillator, which is the so-called Quantum Rabi Model. Quantum Rabi Model allows the exchange of an excitation between these two fundamental physical systems, namely a two-level system and an oscillator [8]. The energy level structure of this 'simple' light-matter interaction is only solvable in terms of special functions,

recently [9]. This motivates the numerical diagonalization of the Rabi system, truncating its infinite dimensional Hilbert space.

The first attempt to solve for Quantum Rabi Model was made by Jaynes and Cummings [10], by applying the rotating wave approximation (RWA), which assumes that the coupling between the subsystems is much smaller than the frequency of the oscillator. Jaynes-Cummings (JC) model allows for the exchange of single excitation between the subsystems and shows Rabi oscillations in a closed subspace of the total Hilbert space with JC doublets. Increasing the interaction strength changes the behaviour dramatically, breaking the JC doublets.

It is possible to have different coupling regimes in the Rabi Model. If the subsystems couple weakly, that implies the losses in the cavity dominate the coupling and prevents the flow of the energy between the subsystems. If they couple strongly, the interaction dominates the losses. In ultrastrong coupling regime, this condition is already fulfilled and the coupling also becomes comparable to the field frequency. Strong coupling in the Rabi Model has been achieved both in atomic systems [11] and in circuit quantum electrodynamic (cQED) systems, with the Cooper pair box [12] and the flux qubit, [13]. The ultrastrong coupling regime was first discussed in [14, 15]. Some theoretical analysis for the Quantum Rabi Model has been performed in the ultrastrong coupling regime, too [1] which points to novel effects. In order to fully understand the physics behind the ultrastrong coupling regime, an intuitive mental picture is required, such as the photon wave packet dynamics in the *parity state chains* of the Quantum Rabi Model in Hilbert space [16]. Some experiments in ultrastrong coupling regime have also been conducted for different systems [17, 18].

The flux qubit is a superconducting qubit that was first introduced in Ref. [19]. Superconducting quantum circuits are more advantageous in some ways than atomic systems in the study of light-matter interaction. For instance, while superconducting systems can be designed with different combinations of qubit and oscillator frequencies, the parameters of the atomic systems are fixed by nature. However, this variability in the artificial system is also a drawback in the fabrication, which might result in unwanted parameter fluctuations, whereas the atomic systems are identical. Another disadvantage of using superconducting qubits is the increased coupling channels to the environment, which causes greater decoherence for the quantum states, [20].

The ultrastrong coupling regime has also been introduced to flux qubit systems, [21] and experiments performed have showed different characteristics of the regime, [22, 23]. However, no one has achieved to apply a Quantum Nondemolition (QND) measurement to a circuit-QED system [24] in the ultrastrong coupling regime, yet. The theoretical

calculation of a QND measurement design for a flux qubit-resonator system in the ultrastrong coupling regime is the main motivation of the current thesis, because such a design is expected to present different energy shifts for different states of the unknown quantum system. In order to achieve this goal, the Rabi Model with an additional weakly coupled resonator, the so-called readout resonator, is proposed to be added to the system and its properties are determined.

Chapter 2

Quantization of the Electromagnetic Fields

The quantization of the electromagnetic field is required when the field is desired to be treated as a quantum-mechanical object. Even though the classical theory of light is quite successful in a great variety of electromagnetic phenomena, e.g. microwave region, due to the small number of photons existing per mode it is necessary to develop a quantum mechanical approach for the optical region of the spectrum, as argued in [25].

Therefore, as an introduction to the background material, first the free space are going to be quantized. Then, the quantization process is going to be applied to a single LC resonator first and then to a continuous structure of LC resonators, namely a transmission line. The quantization of the LC resonator will be utilized in the context of coupling to an artificial spin.

2.1 Quantization of the free electromagnetic field

2.1.1 Classical field equations

Maxwell equations for a charge-free electromagnetic field are,

$$\nabla \times \mathbf{E}(r,t) = -\frac{\partial}{\partial t}\mathbf{B}(r,t), \tag{2.1.1}$$

$$\nabla \times \mathbf{B}(r,t) = \frac{1}{c^2}\frac{\partial}{\partial t}\mathbf{E}(r,t), \tag{2.1.2}$$

$$\nabla \cdot \mathbf{E}(r,t) = 0, \tag{2.1.3}$$

$$\nabla \cdot \mathbf{B}(r,t) = 0. \tag{2.1.4}$$

Let us work with the magnetic vector potential, so that the electric and magnetic fields can be represented in terms of the vector potential.

$$\mathbf{E}(r,t) = -\frac{\partial}{\partial t}\mathbf{A}(r,t), \tag{2.1.5}$$

$$\mathbf{B}(r,t) = \nabla \times \mathbf{A}(r,t). \tag{2.1.6}$$

which satisfies the wave equation,

$$\nabla^2 \mathbf{A}(r,t) - \frac{1}{c^2}\frac{\partial^2}{\partial t^2}\mathbf{A}(r,t) = 0, \tag{2.1.7}$$

with the condition for divergence, $\nabla \cdot \mathbf{A}(r,t) = 0$ in Coulomb gauge. If we Fourier expand the vector potential,

$$\mathbf{A}(r,t) = c_o \sum_k \tilde{A}_{\mathbf{k}}(t) e^{i\mathbf{k}\cdot\mathbf{r}}, \tag{2.1.8}$$

where the constant is chosen as $c_o = \frac{1}{\epsilon_o^{1/2} L^{3/2}}$ for later use and $\mathbf{k}$ wave vectors denote the modes in the field. We will use the transversality condition, which is $\mathbf{k} \cdot \epsilon_{\mathbf{k}s} = 0$, where the numbers $s = 1, 2$ represent two orthogonal linear polarizations of the mode for a real base vector $\epsilon_{\mathbf{k}}$ of the mode $\mathbf{k}$. Now by substituting the Fourier series representation into the wave equation (2.1.7) and utilizing the transversality condition, it can be shown that Fourier coefficients also satisfy the wave equation, so that

$$\tilde{A}_{\mathbf{k}}(t) = \mathbf{c}_{\mathbf{k}} e^{-i\omega t} + \mathbf{c}_{\mathbf{k}}^* e^{i\omega t}. \tag{2.1.9}$$

It is possible to represent the polarization vectors in the coefficients of eq. (2.1.9) by defining,

$$\mathbf{c}_{\mathbf{k}} = \sum_{s=1}^{2} c_{\mathbf{k}s} \epsilon_{\mathbf{k}s}, \tag{2.1.10}$$

where $c_{\mathbf{k}s}$ are weight coefficients of the mode of wave vector $\mathbf{k}$ with a polarization s. When the decomposition (2.1.10) is substituted into the Fourier coefficient equation, (2.1.9), we obtain

$$\tilde{A}_{\mathbf{k}}(t) = \sum_{s=1}^{2} c_{\mathbf{k}s} \epsilon_{\mathbf{k}s} e^{-i\omega t} + \sum_{s=1}^{2} c_{\mathbf{k}s}^* \epsilon_{\mathbf{k}s} e^{i\omega t}. \tag{2.1.11}$$

Then, plugging it into the vector potential equation, (2.1.8) and defining,

$$u_{\mathbf{k}s}(t) = c_{\mathbf{k}s} e^{-i\omega t}, \tag{2.1.12}$$

we obtain a new representation for the vector potential,

$$\mathbf{A}(\mathbf{r},t) = \frac{1}{\epsilon_o^{1/2} L^{3/2}} \sum_{\mathbf{k},s} \left[u_{\mathbf{k}s}(t) \epsilon_{\mathbf{k}s} e^{i\mathbf{k}\cdot\mathbf{r}} + c.c. \right], \tag{2.1.13}$$

where *c.c.* stands for complex conjugate.

2.1.2 Energy of the electromagnetic field

The Hamiltonian of the free electromagnetic field is

$$H = \frac{1}{2} \int \left[\epsilon_o \mathbf{E}^2(\mathbf{r},t) + \frac{1}{\mu_o} \mathbf{B}^2(\mathbf{r},t) \right] d^3\mathbf{r}. \tag{2.1.14}$$

Since we have already derived the equation for the magnetic vector potential, (2.1.13), we can express the electric and magnetic fields by substituting it into eqn's (2.1.5) and (2.1.6). Namely,

$$\mathbf{E}(\mathbf{r},t) = \frac{i}{\epsilon_o^{1/2} L^{3/2}} \sum_{\mathbf{k}} \sum_{s} \omega \left[u_{\mathbf{k}s}(t) \epsilon_{\mathbf{k}s} e^{i\mathbf{k}\cdot\mathbf{r}} - c.c. \right], \tag{2.1.15}$$

$$\mathbf{B}(\mathbf{r},t) = \frac{i}{\epsilon_o^{1/2} L^{3/2}} \sum_{\mathbf{k}} \sum_{s} \left[u_{\mathbf{k}s}(t) \left(\mathbf{k} \times \epsilon_{\mathbf{k}s} \right) e^{i\mathbf{k}\cdot\mathbf{r}} - c.c. \right]. \tag{2.1.16}$$

By using Eqns. (2.1.15) and (2.1.16), one can end up with the energy sum over the modes,

$$H = 2 \sum_{\mathbf{k}} \sum_{s} \omega^2 |u_{\mathbf{k}s}|^2. \tag{2.1.17}$$

In order to apply the quantization, let us define a pair of real canonical variables, $q_{\mathbf{k}s}$ and $p_{\mathbf{k}s}$:

$$q_{\mathbf{k}s}(t) = u_{\mathbf{k}s}(t) + u^*_{\mathbf{k}s}(t), \tag{2.1.18}$$

$$p_{\mathbf{k}s}(t) = -i\omega \left[u_{\mathbf{k}s}(t) - u^*_{\mathbf{k}s}(t) \right]. \tag{2.1.19}$$

Due to the definitions of $u_{\mathbf{k}s}(t)$ variables, (2.1.12), both $q_{\mathbf{k}s}$ and $p_{\mathbf{k}s}$ will oscillate, similar to $u_{\mathbf{k}s}(t)$. When the pair of canonical variables, which satisfy Hamilton's equations [26], are substituted into the Hamiltonian (2.1.17), we finally obtain,

$$H = \frac{1}{2} \sum_{\mathbf{k}} \sum_{s} \left[p^2_{\mathbf{k}s}(t) + \omega^2 q^2_{\mathbf{k}s}(t) \right], \tag{2.1.20}$$

which points to a system of independent (uncoupled) harmonic oscillators for each $\mathbf{k}s$ mode of electromagnetic field. In other words, the analysis lets us model the electromagnetic field by the independent harmonic oscillators for each mode $\mathbf{k}s$ existing in the field.

This is also the key point why we would like to use the quantum harmonic oscillator in the quantization process of the electromagnetic field.

2.1.3 Canonical quantization of the electromagnetic field

The correspondence principle states that a quantum system should predict what the classical formalism predicts in the limit of large quantum numbers, [27]. So by exploiting this principle we can replace the dynamical but classical variables, $p^2_{\mathbf{k}s}(t)$ and $q^2_{\mathbf{k}s}(t)$ by the Hermitian quantum operators $\hat{p}^2_{\mathbf{k}s}(t)$ and $\hat{q}^2_{\mathbf{k}s}(t)$, respectively. Then, the quantized Hamiltonian will be,

$$\hat{H} = \frac{1}{2}\sum_{\mathbf{k}}\sum_{s}\left[\hat{p}^2_{\mathbf{k}s}(t) + \omega^2\hat{q}^2_{\mathbf{k}s}(t)\right], \tag{2.1.21}$$

with the commutation relation $[\hat{q}_{\mathbf{k}s}(t), \hat{p}_{\mathbf{k}'s'}(t)] = i\hbar\delta^3_{\mathbf{k}\mathbf{k}'}\delta_{ss'}$. We will define non-Hermitian operators, namely light quanta annihilation $\hat{a}_{\mathbf{k}s}$ and creation $\hat{a}^\dagger_{\mathbf{k}s}$ operators to use the quantized Hamiltonian, just like in the algebraic analysis of Quantum Harmonic Oscillator, [5]. Here, these the so-called ladder operators might be originated from the factorization of the Hamiltonian, Eq. (2.1.21).

$$\hat{a}_{\mathbf{k}s} = \frac{1}{\sqrt{2\hbar\omega}}\left(\omega\hat{q}_{\mathbf{k}s}(t) + i\hat{p}_{\mathbf{k}s}(t)\right), \tag{2.1.22}$$

$$\hat{a}^\dagger_{\mathbf{k}s} = \frac{1}{\sqrt{2\hbar\omega}}\left(\omega\hat{q}_{\mathbf{k}s}(t) - i\hat{p}_{\mathbf{k}s}(t)\right). \tag{2.1.23}$$

The commutation relation for annihilation and creation operators will be, $\left[\hat{a}_{\mathbf{k}s}(t), \hat{a}^\dagger_{\mathbf{k}'s'}(t)\right] = \delta^3_{\mathbf{k}\mathbf{k}'}\delta_{ss'}$ in Heisenberg picture. The inverse relations will also be used,

$$\hat{q}_{\mathbf{k}s}(t) = \sqrt{\frac{\hbar}{2\omega}}\left(\hat{a}_{\mathbf{k}s}(t) + \hat{a}^\dagger_{\mathbf{k}s}(t)\right), \tag{2.1.24}$$

$$\hat{p}_{\mathbf{k}s}(t) = i\sqrt{\frac{\hbar\omega}{2}}\left(-\hat{a}_{\mathbf{k}s}(t) + \hat{a}^\dagger_{\mathbf{k}s}(t)\right). \tag{2.1.25}$$

Substituting the position and momentum operators, eqs. (2.1.24) and (2.1.25) into the Hamiltonian, eq. (2.1.21),

$$\hat{H} = \frac{1}{2}\sum_{\mathbf{k}}\sum_{s}\hbar\omega\left[\hat{a}_{\mathbf{k}s}(t)\hat{a}^\dagger_{\mathbf{k}s}(t) + \hat{a}^\dagger_{\mathbf{k}s}(t)\hat{a}_{\mathbf{k}s}(t)\right]. \tag{2.1.26}$$

By using the commutation relation, one can show $\hat{a}_{\mathbf{k}s}\hat{a}^\dagger_{\mathbf{k}s} = \hat{a}^\dagger_{\mathbf{k}s}\hat{a}_{\mathbf{k}s} + 1$. Therefore,

$$\hat{H} = \sum_{\mathbf{k}}\sum_{s}\hbar\omega\left[\hat{a}^\dagger_{\mathbf{k}s}(t)\hat{a}_{\mathbf{k}s}(t) + \frac{1}{2}\right], \tag{2.1.27}$$

as expected from a quantum harmonic oscillator. So, the operator $\hat{a}^{\dagger}_{\mathbf{k}s}\hat{a}_{\mathbf{k}s}$ is introduced as the number operator, $\hat{n}_{\mathbf{k}s}$, which represents the population number of the quanta in $\mathbf{k}s$ mode of the electromagnetic field. The number operator is a complete set and the eigenvectors of the number operator are also the eigenvectors of the free field Hamiltonian.

2.1.4 Time dependence of the annihilation and creation operators

The Heisenberg's relation for the time dependence of operators, [5] dictates,

$$\frac{d\hat{O}}{dt} = \frac{i}{\hbar}\left[\hat{H}, \hat{O}\right]. \tag{2.1.28}$$

Then, in order to find out the time dependence of the annihilation and creation operators we can exploit the relation by also using the commutation relation of the annihilation and creation operators.

$$\begin{aligned}
\frac{d\hat{a}_{\mathbf{k}s}}{dt} &= \frac{i}{\hbar}\left[\hat{H}, \hat{a}_{\mathbf{k}s}\right] \\
&= \frac{i}{\hbar}\hbar\omega\left[\sum_{\mathbf{k}'}\sum_{s'}\left(\hat{a}^{\dagger}_{\mathbf{k}'s'}(t)\hat{a}_{\mathbf{k}'s'}(t) + \frac{1}{2}\right), \hat{a}_{\mathbf{k}s}\right] \\
&= i\omega\sum_{\mathbf{k}'}\sum_{s'}\left[\left(\hat{a}^{\dagger}_{\mathbf{k}'s'}\hat{a}_{\mathbf{k}'s'} + \frac{1}{2}\right), \hat{a}_{\mathbf{k}s}\right] \\
&= i\omega\sum_{\mathbf{k}'}\sum_{s'}\left(\hat{a}^{\dagger}_{\mathbf{k}'s'}\hat{a}_{\mathbf{k}'s'}\hat{a}_{\mathbf{k}s} - \hat{a}_{\mathbf{k}s}\hat{a}^{\dagger}_{\mathbf{k}'s'}\hat{a}_{\mathbf{k}'s'}\right) \\
&= i\omega\sum_{\mathbf{k}'}\sum_{s'}\left[\hat{a}^{\dagger}_{\mathbf{k}'s'}, \hat{a}_{\mathbf{k}s}\right]\hat{a}_{\mathbf{k}'s'} \\
&= -i\omega\sum_{\mathbf{k}'}\sum_{s'}\hat{a}_{\mathbf{k}'s'}\delta^{3}_{\mathbf{k}\mathbf{k}'}\delta_{ss'} \\
&= -i\omega\hat{a}_{\mathbf{k}s}.
\end{aligned} \tag{2.1.29}$$

Finally, the differential equation for the ladder operator is

$$\frac{d\hat{a}_{\mathbf{k}s}(t)}{dt} + i\omega\hat{a}_{\mathbf{k}s(t)} = 0. \tag{2.1.30}$$

If we solve it, we obtain

$$\hat{a}_{\mathbf{k}s}(t) = \hat{a}_{\mathbf{k}s}(0)e^{-i\omega t}, \tag{2.1.31}$$

$$\hat{a}^{\dagger}_{\mathbf{k}s}(t) = \hat{a}^{\dagger}_{\mathbf{k}s}(0)e^{i\omega t}. \tag{2.1.32}$$

2.1.5 Final quantized field equations

Since we have the time dependence information of the ladder operators, in section 2.1.4, we can write the final form of the quantized electric and magnetic fields:

$$\mathbf{E}(\mathbf{r},t) = \frac{1}{L^{3/2}} \sum_{\mathbf{k}} \sum_{s} \sqrt{\frac{\hbar\omega}{2\epsilon_o}} \left[i\hat{a}_{\mathbf{k}s}(0)\epsilon_{\mathbf{k}s} e^{i(\mathbf{k}\cdot\mathbf{r}-\omega t)} + h.c. \right] \tag{2.1.33}$$

$$\mathbf{B}(\mathbf{r},t) = \frac{1}{L^{3/2}} \sum_{\mathbf{k}} \sum_{s} \sqrt{\frac{\hbar}{2\omega\epsilon_o}} \left[i\hat{a}_{\mathbf{k}s}(0) \left(\mathbf{k}\times\epsilon_{\mathbf{k}s}\right) e^{i(\mathbf{k}\cdot\mathbf{r}-\omega t)} + h.c. \right] \tag{2.1.34}$$

where h.c. stands for the hermitian conjugate.

2.2 States of electromagnetic field

Some of the states of the quantized electromagnetic field are going to be reviewed in this section.

2.2.1 From number states to multimode number states

We had introduced the number operator for a mode with specific polarization before as,

$$\hat{n}_{\mathbf{k}s} = \hat{n} = \hat{a}^\dagger \hat{a}, \tag{2.2.1}$$

which satisfies the following eigenvalue problem,

$$\hat{n}\left|n\right\rangle = n\left|n\right\rangle. \tag{2.2.2}$$

The number operator has also an orthonormal states, $\left\langle n \,\middle|\, n' \right\rangle = \delta_{nn'}$ and complete $\sum_{n=0}^{\infty} \left|n\right\rangle \left\langle n\right| = 1$. The number state or interchangeably Fock state physically represents a state that contains n photons. It is possible to change the population of photons in that particular mode by applying annihilation and creation operators:

$$\hat{a}\left|n\right\rangle = \sqrt{n}\left|n-1\right\rangle, \tag{2.2.3}$$

$$\hat{a}^\dagger\left|n\right\rangle = \sqrt{n+1}\left|n+1\right\rangle. \tag{2.2.4}$$

Therefore one can build up the number state of an electromagnetic mode from its ground state via repeated action of the creation operators,

$$\left|n\right\rangle = \frac{\left(\hat{a}^\dagger\right)^n}{\sqrt{n!}}\left|0\right\rangle. \tag{2.2.5}$$

When a single mode quantization is generalized to a quantization of an infinite number of modes, e.g. free space, the multimode state of the electromagnetic light is introduced. Due to the independence of field modes, one can simply take the direct product of the number states of each mode in order to build a multimode number state.

$$|\{n\}\rangle = \prod_{\mathbf{k}s} |n_{\mathbf{k},s}\rangle \,. \tag{2.2.6}$$

A multimode number state is an eigenstate of the number operator for any mode $\mathbf{k}$,

$$\hat{n}_{\mathbf{k},s} \,|\{n\}\rangle = n_{\mathbf{k},s} \,|\{n\}\rangle \,, \tag{2.2.7}$$

It is also the eigenstate of the Hamiltonian, Eq. (2.1.27) and similar to the number state, one can also build up a multimode number state from the vacuum state:

$$|\{n\}\rangle = \prod_{\mathbf{k},s} \left(\frac{\left(\hat{a}^{\dagger}_{\mathbf{k},s}\right)^{n_{\mathbf{k},s}}}{\sqrt{n_{\mathbf{k},s}!}} \right) |0\rangle \,. \tag{2.2.8}$$

Finally, a multimode number state is also complete, $\sum_{\{n\}}^{\infty} |\{n\}\rangle \langle\{n\}| = 1$ and orthonormal, $\langle\{n\} \,|\, \{n'\}\rangle = \prod_{\mathbf{k},s} \delta_{n_{\mathbf{k},s} n'_{\mathbf{k},s}}$. An important feature of number states is the expectation value of certain operators. It is straightforward to show that,

$$\begin{aligned} \langle a \rangle &= \langle n| \, a \, |n\rangle \\ &= \sqrt{n} \, \langle n \,|\, n-1\rangle \\ &= 0. \end{aligned} \tag{2.2.9}$$

Similarly for the creation operator,

$$\begin{aligned} \left\langle a^{\dagger} \right\rangle &= \langle n| \, a^{\dagger} \, |n\rangle \\ &= \sqrt{n+1} \, \langle n \,|\, n+1\rangle \\ &= 0, \end{aligned} \tag{2.2.10}$$

due to the orthonormality of the state vectors. Therefore averaging the field operators, e.g. electric field, Eq. (2.1.33) is going to lead to zero for all time, as well, which is not intuitively expected. Because a classical field oscillates sinusoidally, which we can observe different instantaneous values at different times.

2.2.2 The most classical state: The coherent state

Let us first define the coherent state as the eigenstate of the annihilation operator:

$$\hat{a}\,|\alpha\rangle = \alpha\,|\alpha\rangle\,, \qquad \alpha \in \mathbb{C}. \tag{2.2.11}$$

We can utilize the completeness of the number states and represent the eigenstate $|\alpha\rangle$ in terms of number states,

$$|\alpha\rangle = \sum_{n=0}^{\infty} C_n\,|n\rangle\,. \tag{2.2.12}$$

One of the most important motivations of the so called coherent states is their nonvanishing average fields. As also seen in Eq. (2.2.12), such a representation will give us the opportunity to have different number states, which in the end will provide a non-zero average value for the coherent state, $|\alpha\rangle$.

Let us now find the C_n coefficients in the sum, Eq. (2.2.12) via a recursion relation. Apply the annihilation operator to the state and equate it to its Fock state representation.

$$\begin{aligned}\hat{a}\,|\alpha\rangle &= \sum_{n=0}^{\infty} C_n \hat{a}\,|n\rangle \\ &= \sum_{n=0}^{\infty} C_n \sqrt{n}\,|n-1\rangle \\ &= \alpha \sum_{n=0}^{\infty} C_n\,|n\rangle\,,\end{aligned} \tag{2.2.13}$$

which presents a recursion relation,

$$C_n\sqrt{n} = \alpha C_{n-1}. \tag{2.2.14}$$

Then,

$$C_n = \frac{\alpha^n}{\sqrt{n!}} C_0. \tag{2.2.15}$$

By using the orthonormality of number states, $\epsilon^*_{\mathbf{k}s} \cdot \epsilon_{\mathbf{k}s'} = \delta_{ss'}$, one can also easily find the coefficient C_0 as $e^{-0.5|\alpha|^2}$. Then the coherent state will be,

$$|\alpha\rangle = e^{-0.5|\alpha|^2} \sum_{n=0}^{\infty} \frac{\alpha^n}{\sqrt{n!}}\,|n\rangle\,. \tag{2.2.16}$$

Let us now calculate the average value of the electric field in a coherent state. For convenience, let us take the electric field only a specific mode and polarization, so that

$$\mathbf{E}(\mathbf{r},t) = \sqrt{\frac{\hbar\omega}{2L^3\epsilon_o}}\left[i\hat{a}e^{i(\mathbf{k}\cdot\mathbf{r}-\omega t)} - i\hat{a}^\dagger e^{-i(\mathbf{k}\cdot\mathbf{r}-\omega t)}\right]. \tag{2.2.17}$$

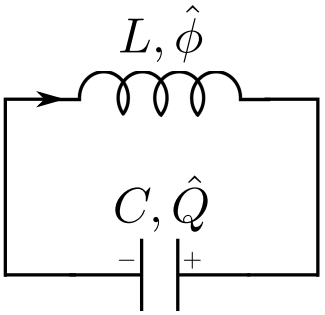

FIGURE 2.1: Schematic of an LC resonator, shown with its quantized canonical variables.

Then averaging it for a coherent state,

$$\begin{aligned}\langle \mathbf{E}(\mathbf{r},t)\rangle &= \langle\alpha|\,\mathbf{E}(\mathbf{r},t)\,|\alpha\rangle \\ &= i\sqrt{\frac{\hbar\omega}{2L^3\epsilon_o}}\left[\alpha e^{i(\mathbf{k}\cdot\mathbf{r}-\omega t)} - \alpha^* e^{-i(\mathbf{k}\cdot\mathbf{r}-\omega t)}\right]. \\ &= 2|\alpha|^2\sqrt{\frac{\hbar\omega}{2L^3\epsilon_o}}\sin\left(\omega t - \mathbf{k}\cdot\mathbf{r}\right)\end{aligned} \tag{2.2.18}$$

So, the expectation value is a sinusoidally oscillating field, as expected.

2.3 Quantization of LC Resonator

Since the interaction between a two-level system and a cavity which is an LC resonator in this case, is going to be analyzed in following chapters, we also need to quantize the cavity field. After the quantization of LC resonator, we will extend the analysis to transmission lines.

2.3.1 Classical Hamiltonian of LC Resonator

Let us first solve the Harmonic Oscillator problem of the LC Resonator classically. A schematic of an LC resonator can be seen in Fig. 2.1. The Hamiltonian will be given as,

$$H = \frac{Q^2}{2C} + \frac{\phi^2}{2L} \tag{2.3.1}$$

where Q is the charge and represents the analogue of the generalized momentum and ϕ is the flux and represents the analogue of the generalized coordinate. The derivation of

the Hamilton's equations from Lagrange principle is given can be seen in the reference, [26]. So, let us use the Hamilton's equations

$$\frac{\partial H(\phi,Q)}{\partial \phi} = -\frac{dQ}{dt}, \qquad \frac{\partial H(\phi,Q)}{\partial Q} = \frac{d\phi}{dt}. \tag{2.3.2}$$

Since $\dfrac{\partial H(\phi,Q)}{\partial \phi} = \dfrac{\phi}{L}$ and $\dfrac{\partial H(\phi,Q)}{\partial Q} = \dfrac{Q}{C}$,

$$\frac{dQ}{dt} = -\frac{\phi}{L}, \tag{2.3.3}$$

$$\frac{d\phi}{dt} = \frac{Q}{C}. \tag{2.3.4}$$

By first differentiating Eq. (2.3.3) and then substituting in Eq. (2.3.4), we obtain

$$\frac{d^2Q}{dt^2} + \frac{Q}{LC} = 0. \tag{2.3.5}$$

which is well-known harmonic oscillator differential equation whose solution is

$$Q(t) = C_1 \sin(\omega t) + C_2 \cos(\omega t) \tag{2.3.6}$$

where $\omega = 1/\sqrt{LC}$ and C_1, C_2 are some arbitrary real constants to be determined by the initial conditions. To conclude, the charge and the flux variables vary sinusoidally with time.

2.3.2 Quantum LC Resonator

The quantization of any electromagnetic field is same as the analysis of the free electromagnetic field. Let us first try to find out the annihilation and creation operators by applying the algebraic analysis of quantum harmonic oscillator to the classical Hamiltonian Eq. (2.3.1). The Hamiltonian classically can be decomposed into,

$$\begin{aligned} H &= \frac{1}{2L}\left(\left(\sqrt{\frac{L}{C}}Q\right)^2 + \phi^2\right) \\ &= \frac{1}{2L}\left(\sqrt{\frac{L}{C}}Q - i\phi\right)\left(\sqrt{\frac{L}{C}}Q + i\phi\right) \end{aligned} \tag{2.3.7}$$

If we quantize these decomposed parts and denote them as the annihilation and creation operators, respectively

$$\hat{a} = \sqrt{\frac{1}{2L}}\left(\sqrt{\frac{L}{C}}\hat{Q} + i\hat{\phi}\right), \tag{2.3.8}$$

$$\hat{a}^\dagger = \sqrt{\frac{1}{2L}}\left(\sqrt{\frac{L}{C}}\hat{Q} - i\hat{\phi}\right). \tag{2.3.9}$$

We can similarly replace the classical variables by the corresponding operators in Eq. (2.3.1) which will give the quantized Hamiltonian.

$$\hat{H} = \frac{\hat{Q}^2}{2C} + \frac{\hat{\phi}^2}{2L}. \tag{2.3.10}$$

where the commutation relation will be $\left[\hat{\phi}, \hat{Q}\right] = i\hbar$. Then finding $\hat{a}^\dagger\hat{a}$,

$$\hat{a}^\dagger\hat{a} = \frac{\hat{Q}^2}{2C} + \frac{\hat{\phi}^2}{2L} - i\frac{1}{2\sqrt{LC}}\left[\hat{Q}, \hat{\phi}\right], \tag{2.3.11}$$

and by exploiting the commutation relation,

$$\hat{a}^\dagger\hat{a} = \frac{\hat{Q}^2}{2C} + \frac{\hat{\phi}^2}{2L} - \frac{1}{2\sqrt{LC}}\hbar, \tag{2.3.12}$$

Since $\omega_{LC} = 1/\sqrt{LC}$, the Hamiltonian will be,

$$\hat{H} = \hbar\omega\left(\hat{a}^\dagger\hat{a} + \frac{1}{2}\right) = \hbar\omega\left(\hat{n} + \frac{1}{2}\right). \tag{2.3.13}$$

We can also represent the field operators in terms of annihilation and creation operators,

$$\hat{Q} = \left(\frac{\hbar}{2}\right)^{1/2}\left(\frac{C}{L}\right)^{1/4}(\hat{a} + \hat{a}^\dagger), \tag{2.3.14}$$

$$\hat{\phi} = -i\left(\frac{\hbar}{2}\right)^{1/2}\left(\frac{L}{C}\right)^{1/4}(\hat{a} - \hat{a}^\dagger). \tag{2.3.15}$$

just like the electric and magnetic fields in the previous section. We define $\sqrt{L/C} = Z_0$, which is introduced as the impedance. This completes the quantization of the LC circuit.

2.4 Quantization of a finite LC Transmission Line

A transmission line (TL) is a 1D distributed microwave circuit where the voltage and current propagate through it as waves, [28]. The quantization analysis of a finite transmission line is necessary in this research, simply because the information from the state of the system under study (a qubit coupled to a resonator) is carried away as a wave in a TL. The analysis in [24] will be followed in order to obtain the quantizations of the voltage and the current waves.

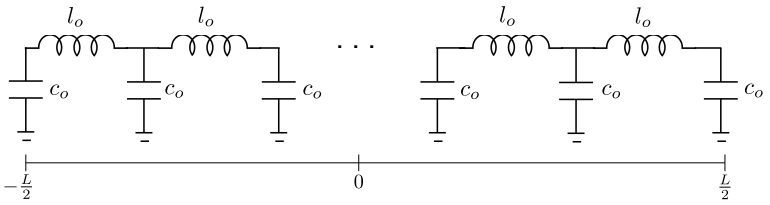

FIGURE 2.2: Schematic of a 1D transmission line, where c_0 is the capacitance per unit length and l_0 is the inductance per unit length.

The voltage on a distributed transmission line is expressed classically as, [28]:

$$V(x,t) = \frac{1}{c_0}\frac{\partial Q(x,t)}{\partial x}. \tag{2.4.1}$$

Therefore, we need to find the position dependence of the charge. Let us first assume that the transmission line has a length L extending from $-L/2$ to $L/2$, as can be depicted in Fig. 2.2 with capacitance per unit length c_0 and inductance per unit length l_0. Then, the charge accumulated at any point x is

$$Q(x,t) = \int_{-L/2}^{x} dx' q(x',t), \tag{2.4.2}$$

where $q(x,t)$ is the charge density in a distributed circuit element. The charge is also the solution of the wave equation

$$\frac{\partial^2 Q}{\partial x^2} = \frac{1}{c^2}\frac{\partial^2 Q}{\partial t^2}, \tag{2.4.3}$$

exposed to boundary conditions $Q(-L/2,t) = Q(L/2,t) = 0$. Since it is a finite transmission line, the solution of the wave equation (2.4.3) can be decomposed into the summations of odd and even bound modes just like a particle in a quantum well. We derived the charge operator in the previous section, Eq. (2.3.14) in the Schrödinger picture. Now, let us restate Eq. (2.3.14) in Heisenberg picture,

$$\hat{Q} = \left(\frac{\hbar}{2}\right)^{1/2}\left(\frac{C}{L}\right)^{1/4}(\hat{a}(t) + \hat{a}^\dagger(t)), \tag{2.4.4}$$

This is the expression for only one mode. However, since TL is a distributed structure, we should sum all modes existing in TL,

$$\begin{aligned}\hat{Q}(x,t) = &\sqrt{\frac{2}{L}}\sum_{k_o=1}^{\infty}\left(\frac{\hbar}{2}\right)^{1/2}\left(\frac{c_0}{l_0}\right)^{1/4}(\hat{a}(t) + \hat{a}^\dagger(t))\cos\left(\frac{k_o\pi x}{L}\right) \\ &+ \sqrt{\frac{2}{L}}\sum_{k_e=1}^{\infty}\left(\frac{\hbar}{2}\right)^{1/2}\left(\frac{c_e}{l_e}\right)^{1/4}(\hat{a}(t) + \hat{a}^\dagger(t))\sin\left(\frac{k_e\pi x}{L}\right).\end{aligned} \tag{2.4.5}$$

Now, invoking Eq. (2.4.1) and using $\omega_0 = 1/\sqrt{l_0 c_0}$,

$$\hat{V}(x,t) = -\sum_{k_o=1}^{\infty} \frac{\hbar\omega_{k_o}}{Lc_0}\frac{k_o\pi}{L}\sin\left(\frac{k_o\pi x}{L}\right)(\hat{a}(t)+\hat{a}^\dagger(t))+\sum_{k_e=2}^{\infty}\frac{\hbar\omega_{k_e}}{Lc_0}\frac{k_e\pi}{L}\cos\left(\frac{k_e\pi x}{L}\right)(\hat{a}(t)+\hat{a}^\dagger(t)). \tag{2.4.6}$$

After obtaining the quantization of the voltage wave, the quantization of current wave is straightforward by using the relation:

$$\hat{V}(x,t) = Z_0\hat{I}(x,t), \tag{2.4.7}$$

we obtain,

$$\hat{I}(x,t) = -\sum_{k_o=1}^{\infty} \frac{\hbar\omega_{k_o}}{LZ_0c_0}\frac{k_o\pi}{L}\sin\left(\frac{k_o\pi x}{L}\right)(\hat{a}(t)+\hat{a}^\dagger(t))+\sum_{k_e=2}^{\infty}\frac{\hbar\omega_{k_e}}{LZ_0c_0}\frac{k_e\pi}{L}\cos\left(\frac{k_e\pi x}{L}\right)(\hat{a}(t)+\hat{a}^\dagger(t)). \tag{2.4.8}$$

Chapter 3

Flux Qubits as Two-level Systems

In this chapter, general treatment of two-level systems is going to be reviewed in the first section. Then in the second section, the flux qubit will be introduced and the treatment is going to be applied to the flux qubit.

3.1 General two-level systems

Two-level systems appear in atomic systems, solid state physics, high energy physics, etc. when two energy levels are close enough to each other that we can ignore the rest of levels. In this way, the physics of level transitions can be confined to the two close levels only.

3.1.1 Energy eigenvalues and normalized eigenvectors of a two-level system under perturbation

Two-level systems can be perturbed by an external factor, e.g. an electric field applied to the system or can be perturbed due to an internal interaction, e.g. a hydrogen ion whose two nuclei are sharing an electron. A perturbative approach can be followed in each case. A perturbation or coupling to an external field can be in general represented by a Hermitian matrix,

$$C = \begin{pmatrix} C_{11} & C_{12} \\ C_{21} & C_{22} \end{pmatrix}, \tag{3.1.1}$$

where C_{11} and C_{22} are real and $C_{12} = C_{21}^*$. When there is no external perturbation, we take the Hamiltonian of the stationary states as H_o,

$$H_o \left|\psi_1\right\rangle = E_1 \left|\psi_1\right\rangle, \tag{3.1.2}$$

$$H_o \left|\psi_2\right\rangle = E_2 \left|\psi_2\right\rangle , \tag{3.1.3}$$

where the basis is orthonormal and complete. In such a case the energy of the system will always be E_1 or E_2 and there will be no interaction between the states. However, introducing a coupling between the states opens the way to analyze dynamical quantum jumps of a two-level system. Due to the linearity of quantum mechanics, we can find the total Hamiltonian by adding perturbation to unperturbed Hamiltonian,

$$H_t = H_o + C = \begin{pmatrix} E_1 + C_{11} & C_{12} \\ C_{12} & E_2 + C_{22} \end{pmatrix}. \tag{3.1.4}$$

With such a Hamiltonian, one should first diagonalize it in order to find the eigenvalues and eigenvectors of the perturbed two-level system. We will use a recipe for this diagonalization as shown in [5]. One can first change the eigenvalue origin of the matrix, Eq. (3.1.4) by decomposing it like

$$H_t = \frac{1}{2}(E_1 + C_{11} + E_2 + C_{22})\mathbb{1} + \frac{1}{2}(E_1 + C_{11} - E_2 - C_{22})\mathbb{K}, \tag{3.1.5}$$

where $\mathbb{K}$ is

$$\mathbb{K} = \begin{pmatrix} 1 & \frac{2C_{12}}{E_1+C_{11}-E_2-C_{22}} \\ \frac{2C_{21}}{E_1+C_{11}-E_2-C_{22}} & 1 \end{pmatrix}, \tag{3.1.6}$$

whose eigenvalues are $k_\pm$ and presents the eigenvalues of the Hamiltonian as

$$E_\pm = \frac{1}{2}(E_1 + C_{11} + E_2 + C_{22}) + \frac{1}{2}(E_1 + C_{11} - E_2 - C_{22})k_\pm. \tag{3.1.7}$$

For convenience, let us define some parameters

$$\tan\theta = \frac{2C_{12}}{E_1 + C_{11} - E_2 - C_{22}}, \tag{3.1.8}$$

$$C_{21} = C_{12}e^{i\phi}, \tag{3.1.9}$$

where $0 \leq \theta < \pi$ and $0 \leq \phi < 2\pi$. Then, the matrix $\mathbb{K}$ will be,

$$\mathbb{K} = \begin{pmatrix} 1 & e^{-i\phi}\tan\theta \\ e^{i\phi}\tan\theta & 1 \end{pmatrix}, \tag{3.1.10}$$

which results in the eigenvalues of $\mathbb{K}$ as,

$$k_\pm = \pm\frac{1}{\cos\theta} \tag{3.1.11}$$

Then, the eigenvalues of the total Hamiltonian will be

$$E_\pm = \frac{1}{2}(E_1 + C_{11} + E_2 + C_{22}) \pm \frac{1}{2}\sqrt{(E_1 + C_{11} - E_2 - C_{22})^2 + 4|C_{12}|^2}. \tag{3.1.12}$$

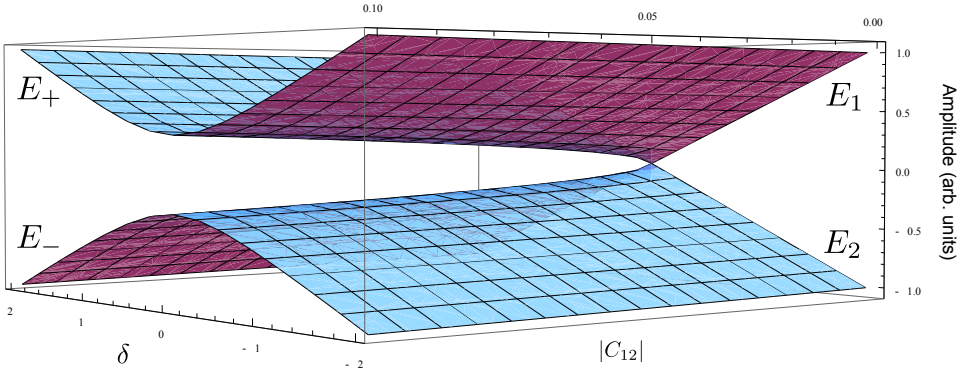

FIGURE 3.1: The energy eigenvalues with respect to δ and the coupling term C_{12}.

Let us now find the normalized eigenvectors by using the $\mathbb{K}$ matrix, Eq. (3.1.10), and its eigenvalues, Eq. (3.1.11):

$$\begin{pmatrix} 1 & e^{-i\phi}\tan\theta \\ e^{i\phi}\tan\theta & 1 \end{pmatrix} \begin{pmatrix} \psi_+ \\ \psi_- \end{pmatrix} = k_\pm \begin{pmatrix} \psi_+ \\ \psi_- \end{pmatrix}, \tag{3.1.13}$$

which will provide the normalized eigenvectors as

$$|\psi_+\rangle = \cos\frac{\theta}{2}e^{-i\phi/2}|\psi_1\rangle + \sin\frac{\theta}{2}e^{i\phi/2}|\psi_2\rangle\,, \tag{3.1.14}$$

$$|\psi_-\rangle = -\sin\frac{\theta}{2}e^{-i\phi/2}|\psi_1\rangle + \cos\frac{\theta}{2}e^{i\phi/2}|\psi_2\rangle\,. \tag{3.1.15}$$

This concludes the diagonalization of the total Hamiltonian. Since non-diagonal terms of the coupling matrix actually represent the coupling, we do not need to have diagonal terms in the coupling matrix C, which lets us to take $C_{11} = C_{22} = 0$. Then, the eigenvalues become

$$E_\pm = \frac{1}{2}(E_1 + E_2) \pm \frac{1}{2}\sqrt{(E_1 - E_2)^2 + 4|C_{12}|^2}, \tag{3.1.16}$$

and the θ parameter

$$\tan\theta = \frac{2C_{12}}{E_1 - E_2}. \tag{3.1.17}$$

The behaviour of the energy eigenvalues can be observed on a plot if we define the detuning parameter $\delta = \frac{1}{2}(E_1 - E_2)$ between the energies, see Fig. 3.1. At the symmetry point ($\delta = 0$), when there is no coupling between the states, the energy levels are degenerate and the levels avoid each other as the coupling increases.

3.1.2 Rabi oscillations of a two-level system

The normalized eigenvectors, Eqs. (3.1.14) and (3.1.15), are also the stationary states of the system. Therefore, the state evolution of an arbitrary wave function will be

$$|\Psi(t)\rangle = c_1 e^{-iE_+ t/\hbar} |\psi_+\rangle + c_2 e^{-iE_- t/\hbar} |\psi_-\rangle . \tag{3.1.18}$$

In order to derive the probability of transition from one state to another, let us assume $|\Psi(0)\rangle = |\psi_1\rangle$, so that the system is at its ground state in the beginning. We will represent the ground state in terms of the stationary states,

$$|\Psi(0)\rangle = |\psi_1\rangle = e^{i\phi/2} \left(\cos\frac{\theta}{2} |\psi_+\rangle - \sin\frac{\theta}{2} |\psi_-\rangle \right) . \tag{3.1.19}$$

The state evolution is then

$$|\Psi(t)\rangle = e^{i\phi/2} \left(\cos\frac{\theta}{2} e^{-iE_+ t/\hbar} |\psi_+\rangle - \sin\frac{\theta}{2} e^{-iE_- t/\hbar} |\psi_-\rangle \right) . \tag{3.1.20}$$

Taking the inner product with the excited state, $|\psi_2\rangle$, will give us the probability of transition:

$$\langle\psi_2 \,|\, \Psi(t)\rangle = e^{i\phi/2} \left(\cos\frac{\theta}{2} e^{-iE_+ t/\hbar} \langle\psi_2 \,|\, \psi_+\rangle - \sin\frac{\theta}{2} e^{-iE_- t/\hbar} \langle\psi_2 \,|\, \psi_-\rangle \right) , \tag{3.1.21}$$

By substituting Eqs. (3.1.14) and (3.1.15) in Eq. (3.1.21),

$$\langle\psi_2 \,|\, \Psi(t)\rangle = e^{i\phi} \cos\frac{\theta}{2} \sin\frac{\theta}{2} \left(e^{-iE_+ t/\hbar} - e^{-iE_- t/\hbar} \right) \tag{3.1.22}$$

Then by some manipulation and using the definition of angles introduced in the previous section, the probability of transition is

$$\begin{aligned} P_{12}(t) &= |\, \langle\psi_2 \,|\, \Psi(t)\rangle \,|^2 \\ &= \sin^2\theta \sin^2 \left(\frac{E_+ - E_-}{2\hbar} t \right) \\ &= \frac{4|C_{12}|^2}{4|C_{12}|^2 + (E_1 - E_2)^2} \sin^2 \left(\sqrt{4|C_{12}|^2 + (E_1 - E_2)^2} \frac{t}{2\hbar} \right) \\ &= \frac{|2C_{12}|^2}{|2C_{12}|^2 + \hbar^2(\omega_1 - \omega_2)^2} \sin^2 \left(\sqrt{|2C_{12}|^2 + \hbar^2(\omega_1 - \omega_2)^2} \frac{t}{2\hbar} \right) \end{aligned} \tag{3.1.23}$$

This equation describes a sinusoidally changing function of time, which is called Rabi formula and describes oscillations between the states of the two-level system.

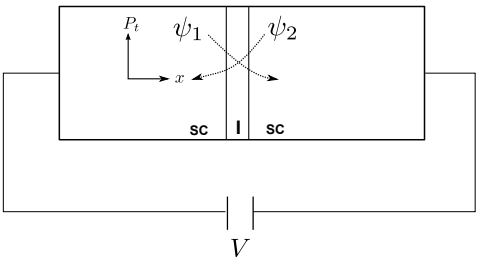

FIGURE 3.2: The physical representation of a Josephson junction.

3.2 Flux Qubits

A flux qubit is a type of superconducting qubit. We are going to apply the general analysis done from the previous section to the particular two-level system which will be used in this research, namely the flux qubit. We will first give a brief introduction about the basic superconducting circuit element, the so-called Josephson junction, which is also the basis of the flux qubit.

3.2.1 Josephson Junction

A Josephson junction is in general a circuit element composed of two superconducting reservoirs connected by a weak link or thin insulating layer. A schematic of the junction can be seen in Fig. 3.2. The role of the thin insulator is to carry out tunnelling of the wave functions at each side, so that the wave function ψ_1 and ψ_2 will leak into the second and first superconducting layers, respectively. This will make possible to write the coupled Schrödinger equations:

$$i\hbar\frac{\partial\psi_1}{\partial t} = U_1\psi_1 + \tau\psi_2 \tag{3.2.1}$$

$$i\hbar\frac{\partial\psi_2}{\partial t} = U_2\psi_2 + \tau\psi_1 \tag{3.2.2}$$

where the $U_{1,2}$ parameters are chemical potential terms which are related to the battery of the circuit, as $U_{1,2} = \pm\frac{qV}{2}$ and τ is the tunnelling rate of the wave functions through the insulating barrier. If we represent the wave function as, $\psi_{1,2} = \sqrt{\rho_1\rho_2}\sin\delta$, where $\delta = \theta_2 - \theta_1$, we obtain

$$\frac{d\rho_{1,2}}{dt} = \pm\frac{2}{\hbar}\Delta\sqrt{\rho_1\rho_2}\sin\delta, \tag{3.2.3}$$

$$\frac{d\theta_{1,2}}{dt} = \frac{\Delta}{\hbar}\sqrt{\frac{\rho_{2,1}}{\rho_{1,2}}}\cos\delta - \frac{qV}{2\hbar}. \tag{3.2.4}$$

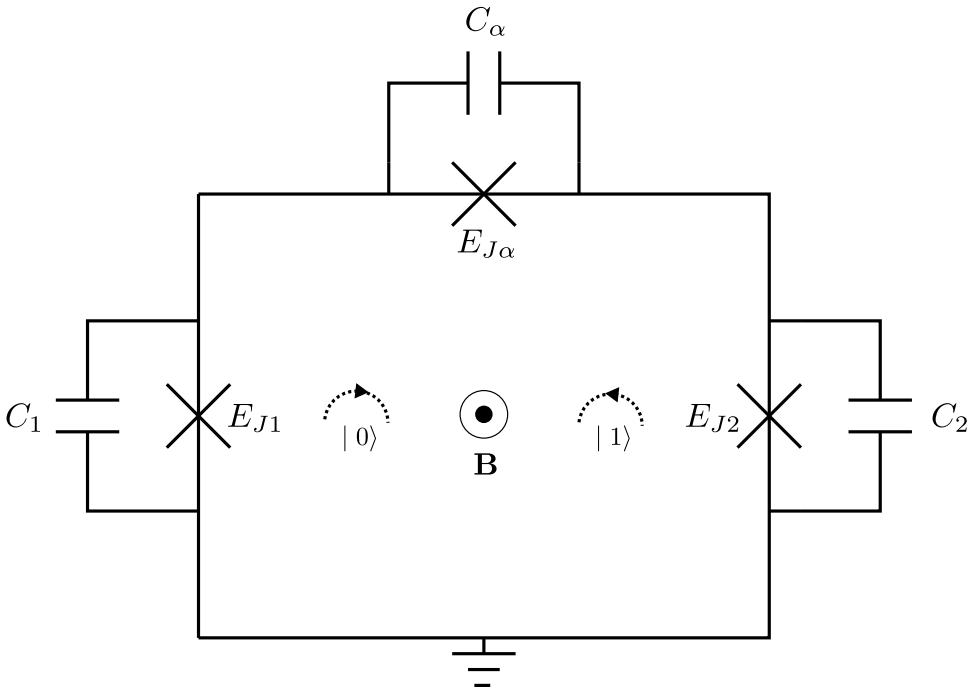

FIGURE 3.3: The circuit represenation of flux qubit.

Equations (3.2.3) and (3.2.4) will give us the Josephson junction equations:

$$I = I_o \sin\delta, \tag{3.2.5}$$

$$\frac{d\delta}{dt} = \frac{2e}{\hbar}V. \tag{3.2.6}$$

where δ is the phase change between the two ends of the element and I_0 is the critical current, which is the maximum amount of current that can flow through a superconducting junction. One can end up with all different kinds of superconducting qubits using Josephson junctions. Josephson junctions provide strong nonlinearity with minimal dissipation to the qubit structures.

3.2.2 Flux Qubit

The flux qubit is a closed superconducting loop which consists of three Josephson junctions connected in series, [19]. A Josephson junction is represented by an ideal Josephson

element and a capacitor connected parallel to it. A circuit diagram of the flux qubit can be seen in Fig. 3.3.

A flux qubit circuit accumulates phase as the current passes by each Josephson junction. Since the superconducting qubits share the same wave function, the phase difference between the wave functions at one point in the circuit should be 2π.

$$\phi_1 - \phi_2 + \phi_\alpha + 2\pi f = 0. \tag{3.2.7}$$

where f is the magnetic frustration and is defined as $f = \frac{\Phi}{\Phi_0}$, Φ is the externally applied magnetic flux and $\Phi_0 = h/2e$ is the flux quantum. The flux induced by the circuit is not taken into account because the flux qubit analyzed here is the first type, [20], which is $L_J/L_s \gg 1$, where L_J is the Josephson junction inductance and L_s is the geometrical loop inductance.

In order to find the total Josephson energy, let us use Eqs. (3.2.5) and (3.2.6) in the integration below for only one Josephson junction,

$$E = \int_0^t IV d\tau = \int_0^t I_o \frac{2e}{\hbar} \sin\delta \frac{d\delta}{d\tau} d\tau = I_o \frac{2e}{\hbar} \int_0^\delta \sin\delta' d\delta' = I_o \frac{2e}{\hbar}(1-\cos\delta) = E_J(1-\cos\delta). \tag{3.2.8}$$

Since we have three Josephson junctions in a flux qubit and one of them has a Josephson energy α multiple of the energy of the others,

$$\begin{aligned} U &= E_J(1 - \cos\delta_1 + 1 - \cos\delta_2 + \alpha - \alpha\cos\delta_\alpha) \\ &= E_J(2 + \alpha - \cos\delta_1 - \cos\delta_2 - \alpha\cos(2\pi f + \delta_1 - \delta_2)), \end{aligned} \tag{3.2.9}$$

by using the phase constraint equation, Eq. (3.2.7). The energy of the flux qubit is a function of two phases, which we can plot as a contour plot, Fig. 3.4 with the parameters $\alpha = 0.8$ and $f = 0.5$. The circular cells show the maxima in the energy, whereas the regions between these cells points out two minima. These minima can be more clearly seen in Fig. 3.5, which indicates there are two stable solutions at symmetry point with a specific value of α. These stable configurations represent the circulating DC currents of opposite direction through the circuit. These currents are called 'persistent currents', [20]. Since the stable solutions simultaneously exist with creating two dips in the potential, it is possible to have a superposition of the persistent currents with probability densities depended on the parameters. All in all, we have a two-level system of flux qubit to use.

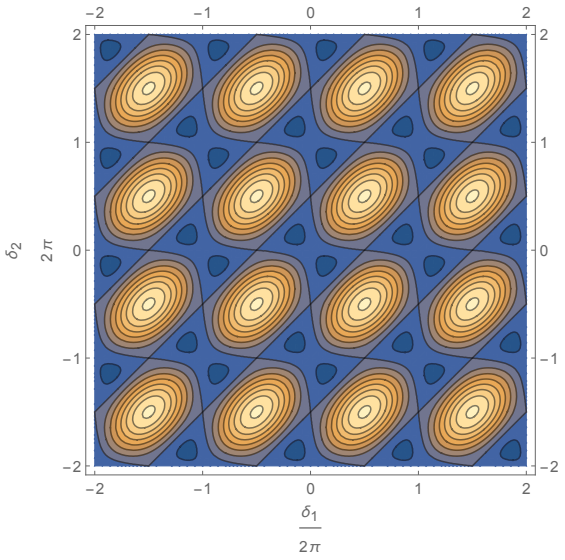

FIGURE 3.4: The contour plot for the energy of the flux qubit with respect to its two different phases when $\alpha = 0.8$ at symmetry point.

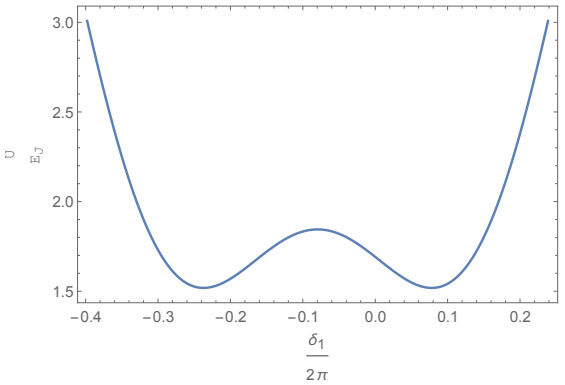

FIGURE 3.5: Two dips seen in the energy plot of the flux qubit which corresponds to two stable solutions.

3.2.3 Hamiltonian of a Flux Qubit under a constant external magnetic field

The Hamiltonian for the flux qubit in the two-level approximation is given by

$$H = \frac{\hbar\Delta}{2}\sigma_x + \frac{\epsilon}{2}\sigma_z, \tag{3.2.10}$$

where ϵ is the magnetic energy of the flux qubit and Δ is the tunnelling rate of the wave functions in the potential energy created by three Josephson junctions in a flux qubit, Fig. 3.5, $\epsilon = 2I_p\Phi_o\left(f - \frac{1}{2}\right)$, where I_p is the persistent current in the flux qubit, Φ_o is the flux quantum and f is the magnetic frustration.

One can diagonalize this Hamiltonian by using the procedure summarized in Section 3.1.1, in order to find its energy eigenvalues and eigenstates. The diagonalization gives

the eigenvalues as

$$\lambda_{1,2} = \mp\frac{1}{2}\sqrt{\epsilon^2 + \Delta^2\hbar^2}, \tag{3.2.11}$$

and the eigenvectors can be chosen as

$$\phi_1 = (\cos\theta/2, \sin\theta/2)\,, \tag{3.2.12}$$

$$\phi_2 = (-\sin\theta/2, \cos\theta/2)\,, \tag{3.2.13}$$

which gives the transformation matrix as

$$T = \begin{pmatrix} \cos\theta/2 & -\sin\theta/2 \\ \sin\theta/2 & \cos\theta/2 \end{pmatrix}, \tag{3.2.14}$$

where $\tan\theta = \hbar\Delta/\epsilon$. It can be shown that $T^{-1}HT$ gives the diagonalized Hamiltonian, Λ:

$$\Lambda = \begin{pmatrix} -\frac{1}{2}\sqrt{\epsilon^2 + \Delta^2\hbar^2} & 0 \\ 0 & \frac{1}{2}\sqrt{\epsilon^2 + \Delta^2\hbar^2} \end{pmatrix}. \tag{3.2.15}$$

A similar plot to Fig. 3.1 for the shifted eigenvalues can be performed, which shows the splitting of energy levels with a non-zero coupling constant.

3.2.4 Hamiltonian of a Flux Qubit under a time dependent external magnetic field

As a second step, we will add a time dependent magnetic field term to the Hamiltonian Eq. (3.2.10), which should be written in terms of the basis of the Hamiltonian Eq. (3.2.15) in the previous section. The driving Hamiltonian looks

$$H_d = A\cos(\omega t)\sigma_z. \tag{3.2.16}$$

Assuming Eq. (3.2.16) is a perturbation, if we apply $T^{-1}H_dT$ we will obtain the driving Hamiltonian in the diagonalized basis of the undriven Hamiltonian, which will be

$$H_d^T = \frac{A\cos\omega t}{\sqrt{\epsilon^2 + \Delta^2\hbar^2}} \begin{pmatrix} \epsilon & -\Delta\hbar \\ -\Delta\hbar & -\epsilon \end{pmatrix}. \tag{3.2.17}$$

Now if we add the undriven Hamiltonian in its eigenbasis and the driving Hamiltonian in the same basis, we will obtain

$$H + H_d = \frac{1}{\sqrt{\epsilon^2 + \Delta^2\hbar^2}} \begin{pmatrix} -\frac{\epsilon^2+\Delta^2\hbar^2}{2} + A\epsilon\cos\omega t & -A\Delta\hbar\cos\omega t \\ -A\Delta\hbar\cos\omega t & \frac{\epsilon^2+\Delta^2\hbar^2}{2} - A\epsilon\cos\omega t \end{pmatrix}. \tag{3.2.18}$$

Then as the last step, we should transform Hamiltonian (3.2.18) to the rotating frame in order to approximate it as a time independent Hamiltonian by using

$$H'_d = UH_dU^\dagger - i\hbar U\frac{\partial U^\dagger}{\partial t}, \tag{3.2.19}$$

where

$$U(t) = e^{-i\omega t\sigma_z/2}, \tag{3.2.20}$$

which could also be written

$$\begin{aligned} U(t) &= \mathbb{I} - i\omega t/2\sigma_z - \frac{1}{2!}(\omega t/2)^2\mathbb{I} + i\frac{1}{3!}(\omega t/2)^3\sigma_z + ... \\ &= \cos(\omega t/2)\mathbb{I} - i\sin(\omega t/2)\sigma_z, \end{aligned} \tag{3.2.21}$$

in terms of cosine and sine Taylor expansions. Therefore,

$$U(t) = \begin{pmatrix} e^{-i\omega t/2} & 0 \\ 0 & e^{i\omega t/2} \end{pmatrix}. \tag{3.2.22}$$

We can differentiate this operator and obtain

$$\frac{dU}{dt} = \frac{-i\omega}{2}\begin{pmatrix} e^{-i\omega t/2} & 0 \\ 0 & -e^{i\omega t/2} \end{pmatrix}. \tag{3.2.23}$$

Multiplying $U^\dagger\frac{dU}{dt}$,

$$U^\dagger\frac{dU}{dt} = \frac{-i\omega}{2}\sigma_z. \tag{3.2.24}$$

Let $H_t = H + H_d$. Multiplying the matrices will give

$$UH_tU^\dagger = \frac{1}{\sqrt{\epsilon^2+\Delta^2\hbar^2}}\begin{pmatrix} -\frac{\epsilon^2+\Delta^2\hbar^2}{2} + A\epsilon\cos\omega t & -Ae^{i\omega t}\Delta\hbar\cos\omega t \\ -Ae^{-i\omega t}\Delta\hbar\cos\omega t & \frac{\epsilon^2+\Delta^2\hbar^2}{2} - A\epsilon\cos\omega t \end{pmatrix}. \tag{3.2.25}$$

Then the Hamiltonian in the rotating frame becomes

$$U_r = \frac{1}{\sqrt{\epsilon^2+\Delta^2\hbar^2}}\begin{pmatrix} -\frac{\epsilon^2+\Delta^2\hbar^2}{2} + A\epsilon\cos\omega t + \frac{\hbar\omega}{2}\sqrt{\epsilon^2+\Delta^2\hbar^2} & -Ae^{i\omega t}\Delta\hbar\cos\omega t \\ -Ae^{-i\omega t}\Delta\hbar\cos\omega t & \frac{\epsilon^2+\Delta^2\hbar^2}{2} - A\epsilon\cos\omega t - \frac{\hbar\omega}{2}\sqrt{\epsilon^2+\Delta^2\hbar^2} \end{pmatrix}. \tag{3.2.26}$$

If we represent $\cos\omega t = \frac{1}{2}\left(e^{i\omega t} + e^{-i\omega t}\right)$, then

$$H_{12} = -\frac{A}{2}\Delta\hbar\frac{(1+e^{2i\omega t})}{\sqrt{\epsilon^2+\Delta^2\hbar^2}}, \tag{3.2.27}$$

$$H_{21} = -\frac{A}{2}\Delta\hbar\frac{(1+e^{-2i\omega t})}{\sqrt{\epsilon^2+\Delta^2\hbar^2}}. \tag{3.2.28}$$

Because the terms with $2\omega t$ angular part will be rotating fast compared to the DC component in Eqs. (3.2.27) and (3.2.28), we can neglect those terms, which is an approximation called the Rotating Wave Approximation, RWA, and will be described fully in the next chapter. Then,

$$H_{12} = H_{21} = -\frac{A}{2}\Delta\hbar\frac{1}{\sqrt{\epsilon^2 + \Delta^2\hbar^2}}. \tag{3.2.29}$$

If we also work at the symmetry point, which implies $\epsilon \to 0$ or $f \to 1/2$,

$$U_r(\epsilon \to 0) = \frac{1}{2}\begin{pmatrix} -\hbar\Delta + \hbar\omega & -A \\ -A & \hbar\Delta - \hbar\omega \end{pmatrix}. \tag{3.2.30}$$

Therefore, as seen from Eq. (3.2.30), the energy terms related to the qubit itself will be at the diagonal of U_r and the magnetic coupling terms will be non-diagonal in the Hamiltonian matrix in rotating frame under RWA.

Chapter 4

Jaynes-Cummings Model of a Flux Qubit-Resonator System

This chapter describes the quantum mechanical model of the interaction between a two-level system and a harmonic oscillator, the so-called Jaynes-Cummings model, [10]. Then we implement the Jaynes-Cummings model in a flux qubit-resonator system both in resonant and dispersive regimes.

4.1 Jaynes-Cummings Model

The Jaynes-Cummings model is a quantum electrodynamical description of the interaction between a two-level system and a single or multi-mode cavity. A schematic of the interaction can be seen in Fig. 4.1. The JC (Jaynes-Cummings) Hamiltonian will be

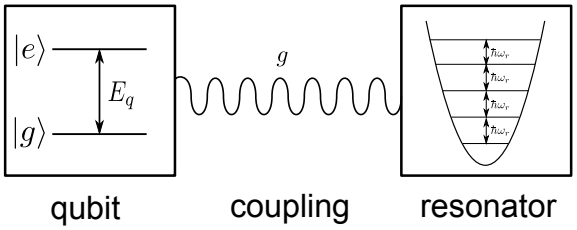

FIGURE 4.1: A schematic for the Jaynes-Cummings Model, represents an interaction between a two-level system and a quantum harmonic oscillator, (schematic copyright [1]).

composed of three parts:

$$\hat{H}_{JC} = \hat{H}_{qb} + \hat{H}_r + \hat{H}_I. \tag{4.1.1}$$

$\hat{H}_{qb}$ is the Hamiltonian of the qubit or two-level system, $\hat{H}_r$ is the Hamiltonian of the resonator and finally $\hat{H}_I$ is the interaction Hamiltonian. The Hamiltonian for the qubit can be written in general as,

$$\hat{H}_{qb} = \frac{1}{2}\hbar\omega_{qb}\hat{\sigma}_z, \tag{4.1.2}$$

where $\hat{\sigma}_z$ is the Pauli Z matrix and the terms in the diagonal represent two independent levels. The Hamiltonian for the resonator is that of a quantum harmonic oscillator, written in terms of annihilation and creation operators,

$$\hat{H}_r = \hbar\omega_r\hat{a}^\dagger\hat{a}, \tag{4.1.3}$$

where we did not take the zero-point energy, simply because we are interested in relative energy values here. Lastly for the interaction Hamiltonian, we should introduce atomic transition operators in a two-level system, which enable the transitions from ground to excited state (or vice versa):

$$\hat{\sigma}_+ \equiv |e\rangle\langle g|, \qquad \hat{\sigma}_- \equiv |g\rangle\langle e|. \tag{4.1.4}$$

The electrodynamic interaction between the two systems can be realized through electric dipole coupling, which can be written as

$$\hat{H}_I = -\hat{\mathbf{d}}\cdot\hat{\mathbf{E}}, \tag{4.1.5}$$

where $\hat{\mathbf{d}}$ is a dipole operator which consists of atomic transition operators, Eq. (4.1.4), and a coupling constant, g. Similarly, from Chapter 2 Section 2.1.5, the quantized electric field can be written in terms of photon creation and annihilation operators. Therefore, when we gather all terms, the full Jaynes-Cummings Hamiltonian (or more generally Rabi model Hamiltonian) becomes

$$\hat{H} = \frac{1}{2}\hbar\omega_{qb}\hat{\sigma}_z + \hbar\omega_r\hat{a}^\dagger\hat{a} + \hbar g(\hat{\sigma}_+ + \hat{\sigma}_-)(\hat{a} + \hat{a}^\dagger). \tag{4.1.6}$$

for a single mode of electric field only, because Jaynes-Cummings model is a single mode spin-boson model.

4.1.1 Rotating-Wave Approximation

In the Heisenberg picture, operators depend on time. If we use the annihilation and creation operators, (2.1.31) and (2.1.32), multiplying with the atomic transition operators,

we obtain for the interaction term:

$$\hat{\sigma}_+\hat{a} \propto e^{i(\omega_{qb}-\omega_r)t} \tag{4.1.7}$$

$$\hat{\sigma}_-\hat{a} \propto e^{-i(\omega_{qb}+\omega_r)t} \tag{4.1.8}$$

$$\hat{\sigma}_+\hat{a}^\dagger \propto e^{i(\omega_{qb}+\omega_r)t} \tag{4.1.9}$$

$$\hat{\sigma}_-\hat{a}^\dagger \propto e^{-i(\omega_{qb}-\omega_r)t} \tag{4.1.10}$$

Equations (4.1.8) and (4.1.9) represent fast rotating terms when compared to the other two terms. Equations (4.1.8) and (4.1.9) are also non-resonant terms in the rotating frame, so that we can apply the so-called rotating wave approximation (RWA) where we drop the fast rotating terms from the Hamiltonian (4.1.6). RWA is only possible under the condition:

$$\frac{g}{\omega_{qb,r}} \ll 1, \tag{4.1.11}$$

where g is the coupling constant between the two-level system and the harmonic oscillator. Such condition implies the non-strong coupling regime. We will analyze the ultra strong coupling regime in next section.

When we take RWA into account, the Hamiltonian (4.1.6) becomes

$$\hat{H} = \frac{1}{2}\hbar\omega_{qb}\hat{\sigma}_z + \hbar\omega_r\hat{a}^\dagger\hat{a} + \hbar g(\hat{a}\hat{\sigma}_+ + \hat{a}^\dagger\hat{\sigma}_-). \tag{4.1.12}$$

This is the Jaynes-Cummings Hamiltonian, [27].

4.1.2 Dressed States: stationary states of JC Hamiltonian

We will state a problem in order to construct the stationary states of Jaynes-Cummings Hamiltonian in this section. The problem will be the determination of the evolution of a time-dependent wave function in the Jaynes-Cummings Hamiltonian when the initial condition given is $|\psi(0)\rangle = |e, n\rangle$, so that the two-level system is in the excited state and the field contains n photons. Even though it is also possible to find the solution by directly solving the Schrödinger equation, we will use the stationary state solution of the Jaynes-Cummings model. Due to the rotating-wave approximation, the interaction between the field and the two-level system is confined to a 2×2 subspace. Then the basis or product states will be,

$$|\psi_1\rangle = |e, n\rangle\,, \tag{4.1.13}$$

$$|\psi_2\rangle = |g, n+1\rangle\,. \tag{4.1.14}$$

In this subspace we can construct the Hamiltonian matrix by using the following relations,

$$\langle e, n \,|\, \hat{\sigma}_z \,|\, e, n \rangle = 1, \tag{4.1.15}$$

$$\langle g, n+1 \,|\, \hat{\sigma}_z \,|\, g, n+1 \rangle = -1, \tag{4.1.16}$$

$$\left\langle g, n+1 \,\middle|\, (\hat{a}\hat{\sigma}_+ + \hat{a}^\dagger \hat{\sigma}_-) \,\middle|\, g, n+1 \right\rangle = 0, \tag{4.1.17}$$

$$\left\langle g, n+1 \,\middle|\, (\hat{a}\hat{\sigma}_+ + \hat{a}^\dagger \hat{\sigma}_-) \,\middle|\, e, n \right\rangle = \sqrt{n+1}. \tag{4.1.18}$$

We will then have the following Hamiltonian matrix,

$$\mathbb{H}^{(n)} = \begin{pmatrix} \hbar n\omega_r + \frac{1}{2}\hbar\omega_{qb} & \hbar g\sqrt{n+1} \\ \hbar g\sqrt{n+1} & \hbar(n+1)\omega_r - \frac{1}{2}\hbar\omega_{qb} \end{pmatrix}, \tag{4.1.19}$$

where $n \geq 0$. Eq. (4.1.19) shows that when $n = 0$ the system, the system still remains coupled even though there is no excitation. If we diagonalize the Hamiltonian (4.1.19) to find the energy eigenvalues and eigenvectors,

$$E_\pm = \hbar\omega_r \left(n + \frac{1}{2}\right) \pm \frac{1}{2}\sqrt{\hbar^2 \left(4g^2(n+1) + \delta^2\right)}, \tag{4.1.20}$$

where $\delta \equiv (\omega_{qb} - \omega_r)$ is the frequency detuning. We can choose the normalized eigenvectors as we did in Chapter 3,

$$|n, +\rangle = \cos(\theta/2)\,|\psi_{1n}\rangle + \sin(\theta/2)\,|\psi_{2n}\rangle\,, \tag{4.1.21}$$

$$|n, -\rangle = -\cos(\theta/2)\,|\psi_{1n}\rangle + \sin(\theta/2)\,|\psi_{2n}\rangle\,, \tag{4.1.22}$$

where,

$$\theta = \tan^{-1}\left(\frac{2g\sqrt{n+1}}{\delta}\right). \tag{4.1.23}$$

These normalized eigenvectors are the dressed states of the Jaynes-Cummings Hamiltonian with the corresponding energy eigenvalues $E_\pm$. Under resonance condition, $\delta = 0$, the dressed states will be represented by superposition of product states as,

$$|n, +\rangle = \frac{1}{\sqrt{2}}\left(|e, n\rangle + |g, n+1\rangle\right), \tag{4.1.24}$$

$$|n, -\rangle = \frac{1}{\sqrt{2}}\left(-|e, n\rangle + |g, n+1\rangle\right). \tag{4.1.25}$$

Let us now apply our initial condition, $|\psi(0)\rangle = |e, n\rangle$, to Eqs. (4.1.24) and (4.1.25). Since this initial state is in $|\psi_{1n}\rangle$, let us write it in terms of dressed states,

$$|\psi(0)\rangle = |\psi_{1n}\rangle = \cos(\theta/2)\,|n, +\rangle - \sin(\theta/2)\,|n, -\rangle\,. \tag{4.1.26}$$

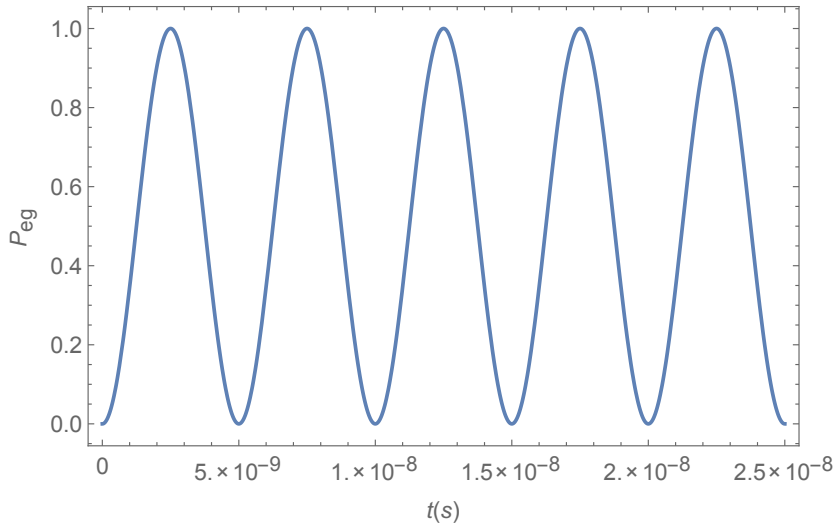

FIGURE 4.2: The Rabi oscillations observed during the transition of state $|e,0\rangle$ to the state $|g,1\rangle$.

Since the dressed states are stationary states, the evolution of the state Eq. (4.1.26) can be in general written by

$$\begin{aligned} |\psi(t)\rangle &= e^{-\frac{i}{\hbar}\hat{H}t}\,|\psi(0)\rangle \\ &= \cos(\theta/2)\,|n,+\rangle\, e^{-\frac{i}{\hbar}E_+t} - \sin(\theta/2)\,|n,-\rangle\, e^{-\frac{i}{\hbar}E_-t}. \end{aligned} \tag{4.1.27}$$

However since we are working on resonance right now, the state will be

$$|\psi(t)\rangle = \frac{1}{\sqrt{2}}\,|n,+\rangle\, e^{-\frac{i}{\hbar}E_+t} - \frac{1}{\sqrt{2}}\,|n,-\rangle\, e^{-\frac{i}{\hbar}E_-t}, \tag{4.1.28}$$

Let us now use the uncoupled state basis representation, Eqs. (4.1.24)-(4.1.25):

$$|\psi(t)\rangle = \frac{1}{2}\left(e^{-\frac{i}{\hbar}E_+t} + e^{-\frac{i}{\hbar}E_-t}\right)|\psi_{1n}\rangle + \frac{1}{2}\left(e^{-\frac{i}{\hbar}E_+t} - e^{-\frac{i}{\hbar}E_-t}\right)|\psi_{2n}\rangle\,. \tag{4.1.29}$$

Substituting the energy eigenvalues,

$$\begin{aligned} |\psi(t)\rangle &= e^{(n+1/2)i\omega_r t}\left(\frac{1}{2}\left(e^{-ig\sqrt{n+1}t} + e^{ig\sqrt{n+1}t}\right)|\psi_{1n}\rangle + \frac{1}{2}\left(e^{-ig\sqrt{n+1}t} - e^{ig\sqrt{n+1}t}\right)|\psi_{2n}\rangle\right) \\ &= e^{(n+1/2)i\omega_r t}\left(\cos(g\sqrt{n+1}t)\,|\psi_{1n}\rangle - i\sin(g\sqrt{n+1}t)\,|\psi_{2n}\rangle\right) \\ &= e^{(n+1/2)i\omega_r t}\left(\cos(g\sqrt{n+1}t)\,|e,n\rangle - i\sin(g\sqrt{n+1}t)\,|g,n+1\rangle\right). \end{aligned} \tag{4.1.30}$$

To find the probability of transition of $|e,n\rangle \to |g,n+1\rangle$:

$$|\,\langle g,n+1\,|\,\psi(t)\rangle\,|^2 = \sin^2(g\sqrt{n+1}t). \tag{4.1.31}$$

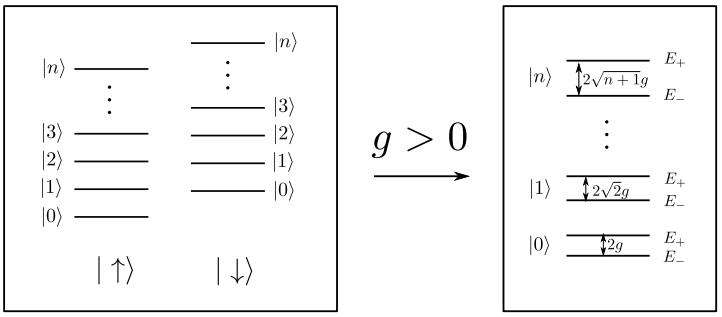

FIGURE 4.3: A schematic which shows the uncoupled Jaynes-Cummings states when $g = 0$ and dressed states when $g > 0$.

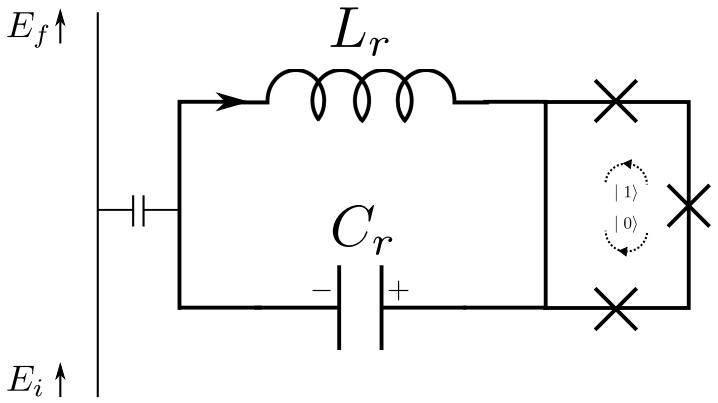

FIGURE 4.4: A circuit schematic which shows the JC model of a flux qubit coupled to an LC resonator.

The probability that a state will stay in its initial state will be,

$$|\langle e, n \,|\, \psi(t)\rangle|^2 = \cos^2(g\sqrt{n+1}t), \tag{4.1.32}$$

which shows oscillations, Fig. 4.2. Since n starts at 0, there is no excitation in the field for the half the period and there is an excitation for the other half. These oscillations are called vacuum Rabi oscillations [28]. The schematic 4.3 shows the uncoupled states when there is no coupling and the formation of the dressed states with a splitting value of the Rabi frequency when the g coupling is on and at resonance.

4.2 Jaynes-Cummings Hamiltonian of Flux Qubit-Resonator System

In a flux qubit-resonator system the coupling is inductive [21] through the interaction of the magnetic field of the resonator and the magnetic moment of the qubit. A schematic

can be seen in Fig. 4.4. The Hamiltonian is

$$H = \frac{\hbar\Delta}{2}\sigma_x + I_p\Phi_o\left(f - \frac{1}{2}\right)\sigma_z + \hbar g\sigma_z(\hat{a} + \hat{a}^\dagger) + \hbar\omega_r\left(\hat{a}^\dagger\hat{a} + \frac{1}{2}\right), \tag{4.2.1}$$

where Δ is the tunnelling rate of the persistent current states in the Josephson potential energy, I_p is the persistent current in the flux qubit, $\Phi_o = h/2e$ is the flux quantum, $f = \Phi_{ext}/\Phi_0$ is the magnetic frustration, g is the coupling strength constant and ω_r is the the frequency of the resonator. Usual experimental values are for $\frac{\omega_r}{2\pi} = \frac{\omega_{qb}}{2\pi} = \frac{\sqrt{\hbar^2\Delta^2+\epsilon^2}}{2\pi} \approx$ 10 GHz, $I_p = 300$ nA and $g/2\pi \approx 100$ MHz, [22] so that $\frac{g}{\omega_{r,qb}} \ll 1$, so that we can apply RWA.

There are some differences between Eq. (4.2.1) and Jaynes-Cummings Hamiltonian, Eq. (4.1.12). The first one is the coupling term which is through magnetic field represented with a Pauli Z operator. The second difference is due to the tunnelling parameter of flux qubit, Δ, which makes the qubit Hamiltonian non-diagonal. So this is the reason we should first diagonalize the qubit Hamiltonian and find its eigenbasis. We will repeat the procedure followed in subsection 3.2.3 for a flux qubit with an applied constant magnetic field. However since the Hamiltonian (4.2.1) consists of two different physical systems, namely a two-level system and a harmonic oscillator, we are going to treat each subsystem individually. The qubit terms read,

$$H_1 = \frac{\hbar\Delta}{2}\sigma_x + I_p\Phi_o\left(f - \frac{1}{2}\right)\sigma_z. \tag{4.2.2}$$

The diagonalization of qubit terms leads to eigenvalues

$$\lambda_{1,2} = \mp\frac{1}{2}\sqrt{4\left(f - \frac{1}{2}\right)^2 I_p^2\Phi_0^2 + \Delta^2\hbar^2} \equiv \mp\frac{\hbar\omega_{qb}}{2}, \tag{4.2.3}$$

and the normalized eigenvectors can be chosen as

$$\phi_1 = (\cos\theta/2, \sin\theta/2)\,, \tag{4.2.4}$$

$$\phi_2 = (-\sin\theta/2, \cos\theta/2)\,, \tag{4.2.5}$$

which gives the transformation matrix:

$$T = \begin{pmatrix} \cos\theta/2 & -\sin\theta/2 \\ \sin\theta/2 & \cos\theta/2 \end{pmatrix}, \tag{4.2.6}$$

where $\tan\theta \equiv \hbar\Delta/\epsilon$ and $\epsilon \equiv 2\left(f-\frac{1}{2}\right)I_p\Phi_o$. It can be shown that $T^{-1}H_1T$ leads to the diagonalized Hamiltonian, Λ:

$$\Lambda = \begin{pmatrix} -\hbar\omega_{qb}/2 & 0 \\ 0 & \hbar\omega_{qb}/2 \end{pmatrix}. \tag{4.2.7}$$

Now we will add the other terms to the diagonalized Hamiltonian. However we first need to represent the other terms in the diagonal basis of Eq. (4.2.2).

$$H_2 = \hbar g\sigma_z(\hat{a}+\hat{a}^\dagger). \tag{4.2.8}$$

Let us apply $T^{-1}H_2T$,

$$H_2^T = \frac{(\hat{a}+\hat{a}^\dagger)g\hbar}{\hbar\omega_{qb}} \begin{pmatrix} 2\left(\frac{1}{2}-f\right)I_p\Phi_0 & -\Delta\hbar \\ -\Delta\hbar & -2\left(\frac{1}{2}-f\right)I_p\Phi_0 \end{pmatrix}, \tag{4.2.9}$$

by using the definition of ϵ let us add the diagonalized Hamiltonian (4.2.7) and Eq. (4.2.9),

$$\Lambda + H_2^T = \begin{pmatrix} \hbar g(\hat{a}+\hat{a}^\dagger)\frac{\epsilon}{\hbar\omega_{qb}} - \frac{\hbar\omega_{qb}}{2} & -\hbar g\frac{\Delta/2}{\omega_{qb}}(\hat{a}+\hat{a}^\dagger) \\ -\hbar g\frac{\Delta/2}{\omega_{qb}}(\hat{a}+\hat{a}^\dagger) & -\hbar g(\hat{a}+\hat{a}^\dagger)\frac{\epsilon}{\hbar\omega_{qb}} + \frac{\hbar\omega_{qb}}{2} \end{pmatrix}. \tag{4.2.10}$$

Then as the last step we should add the last term of the Hamiltonian (4.2.1), which is $\hbar\omega_r\left(\hat{a}^\dagger\hat{a}+\frac{1}{2}\right)$, so it applies the identity matrix on the qubit. Then,

$$H_3 = \begin{pmatrix} \hbar\omega_r\left(\hat{a}^\dagger\hat{a}+\frac{1}{2}\right) & 0 \\ 0 & \hbar\omega_r\left(\hat{a}^\dagger\hat{a}+\frac{1}{2}\right) \end{pmatrix}. \tag{4.2.11}$$

If we add the matrix Eq. (4.2.11) to the Hamiltonian (4.2.10),

$$H = \begin{pmatrix} \hbar g(\hat{a}+\hat{a}^\dagger)\frac{\epsilon}{\omega_{qb}} - \frac{\hbar\omega_{qb}}{2} + \hbar\omega_r\left(\hat{a}^\dagger\hat{a}+\frac{1}{2}\right) & -\hbar g\frac{\Delta}{\omega_{qb}}(\hat{a}+\hat{a}^\dagger) \\ -\hbar g\frac{\Delta}{\omega_{qb}}(\hat{a}+\hat{a}^\dagger) & -\hbar g(\hat{a}+\hat{a}^\dagger)\frac{\epsilon}{\omega_{qb}} + \frac{\hbar\omega_{qb}}{2} + \hbar\omega_r\left(\hat{a}^\dagger\hat{a}+\frac{1}{2}\right) \end{pmatrix}. \tag{4.2.12}$$

So we obtain the total Hamiltonian as

$$\hat{H} = \left(-\hbar g(\hat{a}+\hat{a}^\dagger)\frac{\epsilon}{\omega_{qb}} + \frac{\hbar\omega_{qb}}{2}\right)\sigma_z - \hbar g\frac{\Delta}{\omega_{qb}}\sigma_x(\hat{a}^\dagger+\hat{a}) + \hbar\omega_r\left(\hat{a}^\dagger\hat{a}+\frac{1}{2}\right). \tag{4.2.13}$$

Let us define $\frac{\epsilon}{\hbar\omega_{qb}} \equiv \cos\theta$ and $\frac{\Delta}{\omega_{qb}} \equiv \sin\theta$, then

$$\hat{H} = -\hbar g(\hat{a}+\hat{a}^\dagger)\cos\theta\sigma_z + \frac{\hbar\omega_{qb}}{2}\sigma_z - \hbar g\sin\theta\sigma_x(\hat{a}^\dagger+\hat{a}) + \hbar\omega_r(\hat{a}^\dagger\hat{a}+\frac{1}{2}). \tag{4.2.14}$$

Because of the magnetic energy in the first term in Eq. (4.2.14), the first term is negligible compared to other terms. So we can eliminate it and have,

$$\hat{H} = \frac{\hbar\omega_{qb}}{2}\sigma_z - \hbar g \sin\theta \sigma_x(\hat{a}^\dagger + \hat{a}) + \hbar\omega_r \left(\hat{a}^\dagger\hat{a} + \frac{1}{2}\right), \tag{4.2.15}$$

Lastly, in the Heisenberg picture the operators depend on time and $\hat{a} = \hat{a}(0)e^{-i\omega_r t}$ and $\hat{a}^\dagger = \hat{a}^\dagger(0)e^{i\omega_r t}$. Assuming that $\frac{g}{\omega_r} \ll 1$, the RWA can be applied to the coupling term. Then,

$$\hat{H} = \frac{\hbar\omega_{qb}}{2}\sigma_z - \hbar g \sin\theta \left(\hat{\sigma}_-\hat{a}^\dagger + \hat{\sigma}_+\hat{a}\right) + \hbar\omega_r \left(\hat{a}^\dagger\hat{a} + \frac{1}{2}\right), \tag{4.2.16}$$

which is the flux qubit-resonator Hamiltonian in Jaynes-Cummings form. Now in order to form the Hamiltonian matrix, let us define,

$$\psi_1 = |g, n+1\rangle, \tag{4.2.17}$$

$$\psi_2 = |e, n\rangle. \tag{4.2.18}$$

By using the following equalities,

$$\langle g, n+1 \,|\, e, n\rangle = 0, \tag{4.2.19}$$

$$\langle g, n+1 \,|\, g, n\rangle = \langle e, n+1 \,|\, e, n\rangle = 0, \tag{4.2.20}$$

$$\begin{aligned} \langle e, n \,|\, \sigma_z \,|\, e, n\rangle &= \langle e, n \,|\, (|e\rangle\langle e| - |g\rangle\langle g|) \,|\, e, n\rangle \\ &= \langle e, n \,|\, |e\rangle\langle e| \,|\, e, n\rangle - \langle e, n \,|\, |g\rangle\langle g| \,|\, e, n\rangle \\ &= \langle e, n \,|\, e, n\rangle - 0 \\ &= 1. \end{aligned} \tag{4.2.21}$$

Similarly for,

$$\langle g, n \,|\, \sigma_z \,|\, g, n\rangle = -1. \tag{4.2.22}$$

Repeating it for the interaction term:

$$\begin{aligned} \left\langle g, n \left| \hat{H}^I \right| g, n \right\rangle &= -\hbar g \sin\theta \left\langle g, n \left| (\sigma_+\hat{a} + \sigma_-\hat{a}^\dagger) \right| g, n \right\rangle \\ &= -\hbar g \sin\theta \left(\langle g, n \,|\, \sigma_+\hat{a} \,|\, g, n\rangle + \left\langle g, n \left| \sigma_-\hat{a}^\dagger \right| g, n \right\rangle\right) \\ &= -\hbar g \sin\theta(\langle g, n \,|\, e, n-1\rangle + 0) \\ &= 0, \end{aligned} \tag{4.2.23}$$

by the Eq. (4.2.19) and the fact that the energy levels of the qubit span a 2-dimensional space so that any operator which intends to take the system out of this reduced Hilbert

space has zero expectation value. Similarly for,

$$\left\langle e,n \left| \hat{H}^I \right| e,n \right\rangle = 0. \tag{4.2.24}$$

Let us also inspect,

$$\begin{aligned}\left\langle g,n+1 \left| \hat{H}^I \right| e,n \right\rangle &= -\hbar g \sin\theta \left\langle g,n+1 \left| (\sigma_+\hat{a} + \sigma_-\hat{a}^\dagger) \right| e,n \right\rangle \\ &= -\hbar g \sin\theta (\langle g,n+1 \,|\, \sigma_+\hat{a} \,|\, e,n\rangle + \left\langle g,n+1 \left| \sigma_-\hat{a}^\dagger \right| e,n \right\rangle) \\ &= -\hbar g \sin\theta (0 + \sqrt{n+1}\,\langle g,n+1 \,|\, g,n+1\rangle) \\ &= -\hbar g \sin\theta \sqrt{n+1},\end{aligned} \tag{4.2.25}$$

$$\begin{aligned}\left\langle e,n \left| \hat{H}^I \right| g,n+1 \right\rangle &= -\hbar g \sin\theta \left\langle e,n \left| (\sigma_+\hat{a} + \sigma_-\hat{a}^\dagger) \right| g,n+1 \right\rangle \\ &= -\hbar g \sin\theta (\langle e,n \,|\, \sigma_+\hat{a} \,|\, g,n+1\rangle + \left\langle e,n \left| \sigma_-\hat{a}^\dagger \right| g,n+1 \right\rangle) \\ &= -\hbar g \sin\theta (\sqrt{n+1}\,\langle e,n \,|\, e,n\rangle + 0) \\ &= -\hbar g \sin\theta \sqrt{n+1}.\end{aligned} \tag{4.2.26}$$

Due to the orthogonality of number states (similar for excited state, as well):

$$\left\langle g,n \left| \hat{H}^I \right| g,n+1 \right\rangle = 0, \tag{4.2.27}$$

$$\langle g,n \,|\, \sigma_z \,|\, g,n+1\rangle = 0. \tag{4.2.28}$$

Now we can construct the matrix for our Hamiltonian:

$$\hat{H} = \begin{pmatrix} \ddots & & & \\ & \frac{\hbar\omega_{qb}}{2} + \Omega_r(n) & -\hbar g \sin\theta\sqrt{n+1} & \\ & -\hbar g \sin\theta\sqrt{n+1} & -\frac{\hbar\omega_{qb}}{2} + \Omega_r(n+1) & \\ & & & \ddots \end{pmatrix}. \tag{4.2.29}$$

where $\Omega_r(n) = \hbar\omega_r\left(n + \frac{1}{2}\right)$. If we diagonalize this matrix, we will obtain different eigenvalues in the general form,

$$E_{\pm,n} = (n+1)\hbar\omega_r \pm \frac{1}{2}\sqrt{(n+1)\left(\frac{2\hbar g\Delta}{\omega_{qb}}\right)^2 + \hbar^2(\omega_{qb} - \omega_r)^2}, \tag{4.2.30}$$

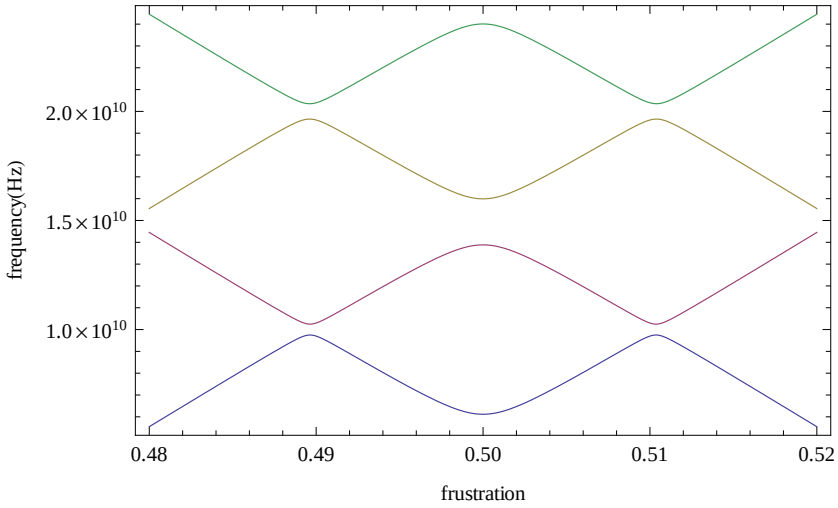

FIGURE 4.5: Energy levels with respect to magnetic field frustration in the qubit when up to states with two photons exist in the resonator with $g = 0.05\omega_r$, vertical axis is frequency in Hz. Pink: $E_{0,-}$, blue: $E_{0,+}$, green: $E_{1,-}$ and brown: $E_{1,+}$.

where n is the excitation number. Using $\delta = \omega_{qb} - \omega_r$, write Eq. 4.2.30 in terms of detuning parameter as,

$$E_{\pm,n} = (n+1)\hbar\omega_r \pm \frac{\hbar}{2}\sqrt{(n+1)\left(\frac{2g\Delta}{\omega_{qb}}\right)^2 + \delta^2}. \tag{4.2.31}$$

where $\delta = \frac{1}{\hbar}\sqrt{4\left(f-\frac{1}{2}\right)^2 I_p^2\Phi_0^2 + \Delta^2\hbar^2} - \omega_r$, explicitly.

Under zero coupling and at resonance, the energy levels are degenerate as $E_{\pm,n} = (n+1)\hbar\omega_r$ for both ground and excited states of the qubit. Increasing the coupling breaks the degeneracy and the dressed states of the Jaynes-Cummings Hamiltonian form with the following eigenvalues, $E_{\pm,n} = (n+1)\hbar\omega_r \pm \hbar g\sqrt{n+1}\dfrac{\Delta}{\omega_{qb}}$. This process was also depicted in Fig. 4.3.

We can plot the energy levels under nonzero and zero couplings, Figs. 4.5 and 4.6. As can be observed when the coupling strength is nonzero, the energy levels avoid each other and the degeneracies disappear, as expected.

4.3 Jaynes-Cummings Model in Dispersive Regime

The parameter the so-called *detuning* was introduced in previous section during the analysis of Jaynes-Cummings Model as the difference between the qubit and resonator frequency:

$$\delta = \omega_{qb} - \omega_r. \tag{4.3.1}$$

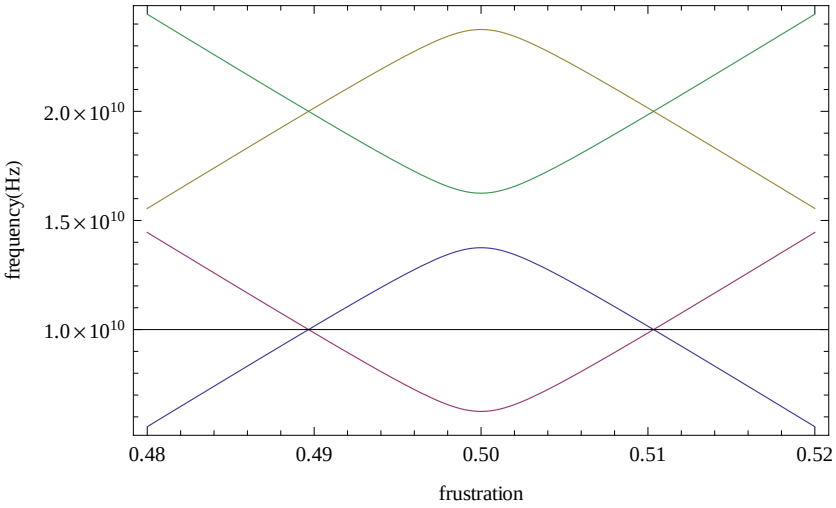

FIGURE 4.6: The energy levels with respect to magnetic frustration when two photons exist in the resonator with $g = 0$, vertical axis is frequency in Hz. Pink: $E_{0,-}$, blue: $E_{0,+}$, green: $E_{1,-}$ and brown: $E_{1,+}$.

When there is a large detuning, $2g\sqrt{n+1}/\delta \ll 1$, we can expand Eq. (4.2.31) as

$$\begin{aligned} E^d_{\pm} &= (n+1)\hbar\omega_r \pm \frac{\hbar}{2}\delta\sqrt{(n+1)\left(\frac{2g\Delta}{\omega_{qb}\delta}\right)^2 + 1} \\ &= (n+1)\hbar\omega_r \pm \frac{\hbar}{2}\delta\left(1 + \frac{1}{2}(n+1)\left(\frac{2g\Delta}{\omega_{qb}\delta}\right)^2\right) \\ &= (n+1)\hbar\omega_r \pm \left(\frac{\delta\hbar}{2} + \hbar(n+1)\frac{g^2}{\delta}\frac{\Delta^2}{\omega^2_{qb}}\right) \\ &= \hbar(n+1)\left(\omega_r \pm \frac{g^2}{\delta}\frac{\Delta^2}{\omega^2_{qb}}\right) \pm \frac{\delta\hbar}{2}. \end{aligned} \tag{4.3.2}$$

As observed from the expansion, a factor of $\frac{g^2}{\delta}\frac{\Delta^2}{\omega^2_{qb}}$ will be subtracted from the resonator frequency when the qubit is in the ground state and added to the resonator frequency for the excited state of the qubit. This shift introduced to the resonator frequency is called Stark shift which can be observed in the spectrum of the resonator.

One can also obtain the same shift by applying a unitary transformation [24],

$$U = e^{\frac{g}{\delta}(a\sigma_+ - a^\dagger\sigma_-)}, \tag{4.3.3}$$

to the Hamiltonian (4.2.16) and expanding to second order in g/δ,

$$H^d_{JC} \approx \hbar\left(\omega_r + \frac{g^2}{\delta}\sin^2\theta\sigma_z\right)a^\dagger a + \frac{\hbar}{2}\left(\omega_{qb} + \frac{g^2}{\delta}\sin^2\theta\right)\sigma_z. \tag{4.3.4}$$

The shifts in this expression can be interpreted in two ways. The first one shows a shift in the frequency of the resonator depending on the state of the qubit, so that the dispersive coupling between the systems affects the resonator frequency. The second one shows a shift in the frequency of the qubit caused by the dispersive coupling to the resonator that increases with the photon number. For the qubit, there is always a shift observed when compared to the case where $g = 0$ which is independent of photon number, $g^2/2\delta$. It is the Lamb shift, which comes from the vacuum fluctuations of zero point energy of the resonator.

Quantum coherence of the qubit state is an important parameter in a quantum system, which means that the information in the qubit system is protected from the fluctuations of the environment. Driving a qubit in the dispersive regime is a way to readout the state of the atom or qubit under weak coupling before the coherence is lost. This will be further analysed in Chapter 6.

Chapter 5

Quantum Rabi Model in a Superconducting Circuit

The flux qubit-resonator Hamiltonian in the ultrastrong coupling regime is analyzed in this chapter. The ultrastrong coupling regime requires $g \approx \omega_{qb,r}$, which invalidates the application of Rotating Wave Approximation to the problem. Therefore all of the interaction terms are taken into account and the resulting model is called the Quantum Rabi Model, [7].

5.1 Ultrastrong Coupling Regime

In the previous section, the RWA allowed us to reduce the Rabi model to JC model, which is exactly solvable. However, when the RWA breaks down the full Hamiltonian is not box-diagonal and one cannot reach an analytical solution, except recently [9].

When the coupling of the qubit to the resonator becomes comparable to the qubit and resonator energies, the subsystems do not evolve individually, but as a whole single system. This creates a completely different conceptual picture than the Jaynes-Cummings model of single exchanged excitation between the two subsystems. The operators $\hat{a}\hat{\sigma}_+$ and $\hat{a}^\dagger\hat{\sigma}_-$ conserve the number of excitations between the individual subsystems when the subsystems are weakly coupled. As we increase the coupling strength, the other two operators, $\hat{a}\hat{\sigma}_-$ and $\hat{a}^\dagger\hat{\sigma}_+$ also start to take a part in the excitation dynamics of the ultrastrongly coupled quantum system. The excitation exchange mechanism that these operators provide to the system is due to the extra energy introduced to the system by the coupling strength which is comparable to the energy of the subsystems.

There is substantial theoretical research conducted on the quantum Rabi model which presents valuable insights about the nature of the structure of the system [9, 14–16]. Solving the Rabi Model Hamiltonian numerically and analysing the evolution of the energy levels under different detuning parameters shows a clear entanglement between the qubit and resonator states, [1, 9]. One can obtain the complete eigenstates of the system with specific detuning parameters under adiabatic constraints [1]. There are also recent experiments conducted in ultrastrong coupling regime for superconducting qubits [22, 23] and for different systems, [17, 18].

A more intuitive picture is given in terms of *the parity chains of states* [16] . A parity operator,

$$\Pi = -\sigma_z(-1)^{b^\dagger b}, \tag{5.1.1}$$

is used to express the quantum Rabi Model Hamiltonian in this parity basis, $|p, n_b\rangle$ where $p = \pm 1$ and $b^\dagger b\,|n_b\rangle = n_b\,|n_b\rangle$ with $|n_b\rangle$ is the number state. Also, $b = \sigma_x a$ where a is the annihilation operator in the Rabi Hamiltonian, (4.2.15), so that b is the annihilation operator in the parity basis. This basis might be useful to visualize the dynamics of excitations in Hilbert space by expressing two possible parity chains,

$$|g0\rangle \leftrightarrow |e1\rangle \leftrightarrow |g2\rangle \leftrightarrow |e3\rangle \leftrightarrow \ldots \quad (p = 1), \tag{5.1.2}$$

$$|e0\rangle \leftrightarrow |g1\rangle \leftrightarrow |e2\rangle \leftrightarrow |g3\rangle \leftrightarrow \ldots \quad (p = -1). \tag{5.1.3}$$

The parity chains cannot intersect, so that they evolve independent from each other. By using appropriate operators, one can climb up or down to any possible state in that specific chain. Then, by transforming the Rabi Hamiltonian to the parity basis, one can obtain the collapse-revival picture of the populations in the parity chains [16].

5.2 Numerical solution of the Quantum Rabi Model

The flux qubit-resonator Hamiltonian is given by,

$$\hat{H} = \frac{\hbar\Delta}{2}\sigma_x + I_p\Phi_o\left(f - \frac{1}{2}\right)\sigma_z + \hbar g\sigma_z(\hat{a} + \hat{a}^\dagger) + \hbar\omega_r\left(\hat{a}^\dagger\hat{a} + \frac{1}{2}\right). \tag{5.2.1}$$

We will first express Eq. (5.2.1) in tensors products:

$$\hat{H} = \frac{\hbar\Delta}{2}(\sigma_x \otimes \mathbb{I}_n) + I_p\Phi_o\left(f - \frac{1}{2}\right)(\sigma_z \otimes \mathbb{I}_n) + \hbar g(\sigma_z \otimes (\hat{a} + \hat{a}^\dagger)) + \hbar\omega_r\left(\mathbb{I}_{qb} \otimes \left(\hat{a}^\dagger\hat{a} + \frac{1}{2}\right)\right). \tag{5.2.2}$$

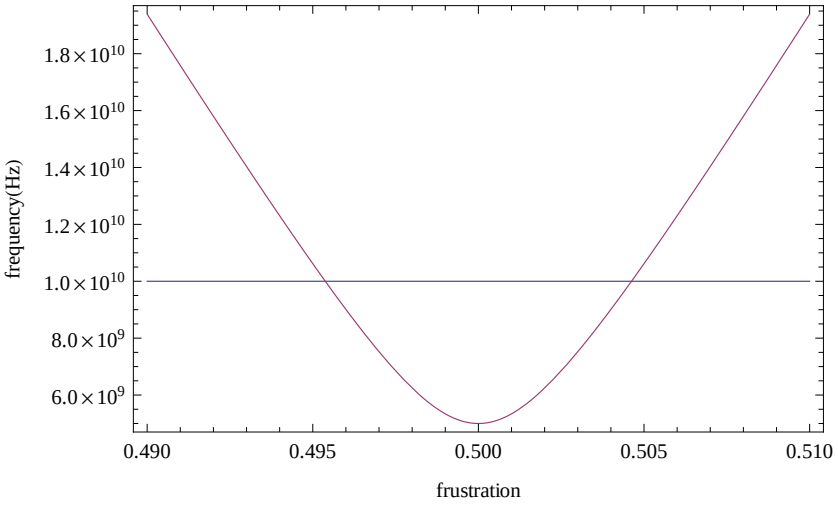

FIGURE 5.1: The difference between energy levels of QRM with respect to magnetic field frustration in the qubit with $g = 0$. The vertical axis is frequency in Hz. Pink is the difference between the ground state and first excited state energies, blue is the difference between the ground state and the second excited state energies. 7 photon states are used for this calculation.

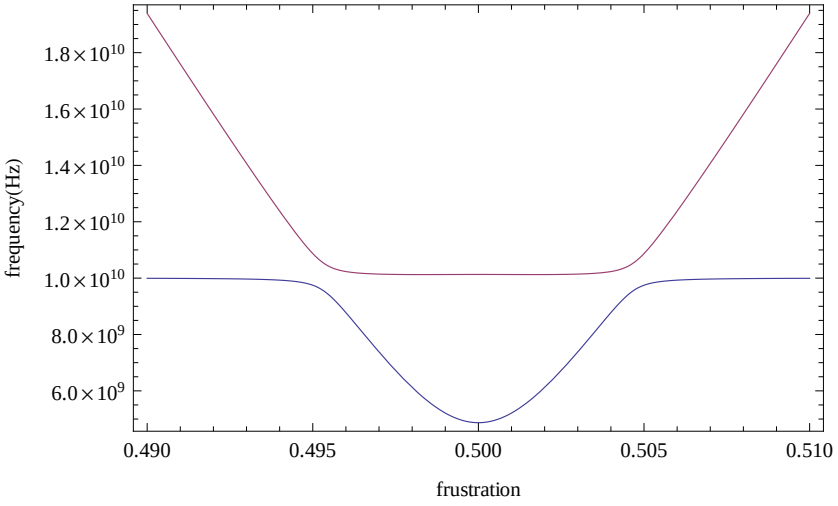

FIGURE 5.2: The difference between energy levels of QRM with respect to magnetic field frustration in the qubit with $g = \omega_r$. The vertical axis is frequency in Hz. Blue is the difference between the ground state and first excited state energies, pink is the difference between the ground state and the second excited state energies. 7 photon states are used for this calculation.

where all the parameters are defined in Section 4.2 in Chapter 4. As a note for the tensor products, the left operator will belong to qubit Hilbert space and the right operator to the resonator Hilbert space. Since the qubit is a two-level system, its Hilbert space has dimension 2, while the dimension of the Hilbert space of the resonator is the dimension of the Fock space of the resonator.

Solving Eq. (5.2.2) with $g = 0$ coupling leads to the spectrum plot in Fig. 5.1. Increasing the coupling to a non-zero value creates the vacuum Rabi splitting of the energy levels,

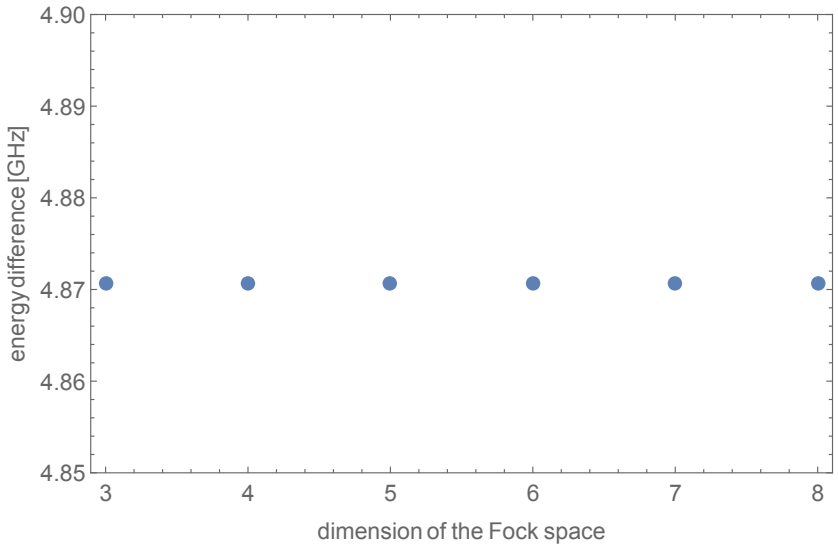

FIGURE 5.3: The dependence of the energy difference between the ground state $|g0\rangle \rightarrow |G\rangle$ and the first excited state $|e0\rangle \rightarrow |E\rangle_q$ on the dimension of the Fock space when $g = 0.1\omega_r$ and $f = 0.5$ with $\omega_r/2\pi = 10$ GHz and $\omega_{qb}/2\pi = 5$ GHz.

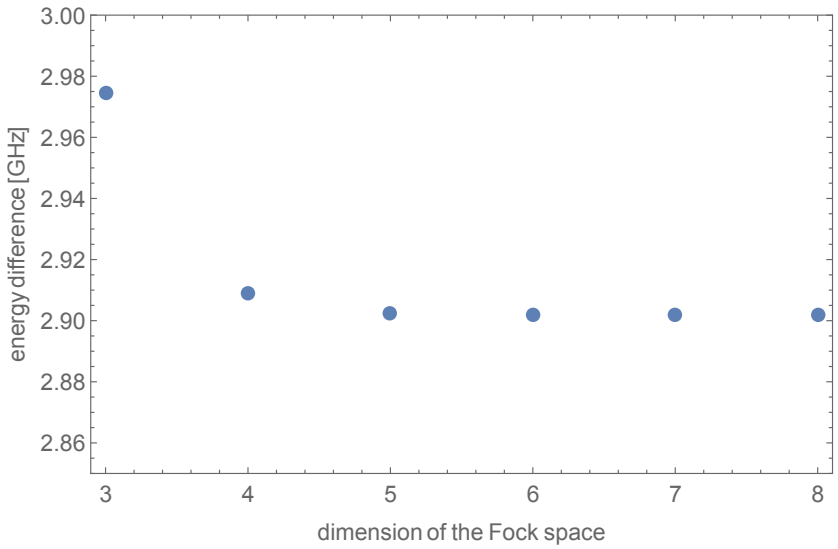

FIGURE 5.4: The dependence of the energy difference between the ground state $|g0\rangle \rightarrow |G\rangle$ and the first excited state $|e0\rangle \rightarrow |E\rangle_q$ on the dimension of the Fock space when $g = 0.1\omega_r$ and $f = 0.5$ with $\omega_r/2\pi = 10$ GHz and $\omega_{qb}/2\pi = 5$ GHz.

(Fig. 5.2).

In order to see the dependence of the model on the coupling strength, we will fix the frustration $f = 0.5$, which is the symmetry point of the qubit. It can be shown that the energy difference between the ground and first excited states of the coupled system is a function of the dimension of Fock space being used, Figs. 5.3-5.5. As seen in the previous section of ultrastrong coupling regime, the parity chains of Rabi Model are infinite, which shows the infinite dimension of the Hilbert space used in the process. Solving the Hamiltonian numerically forces to take a finite dimension of the Fock space

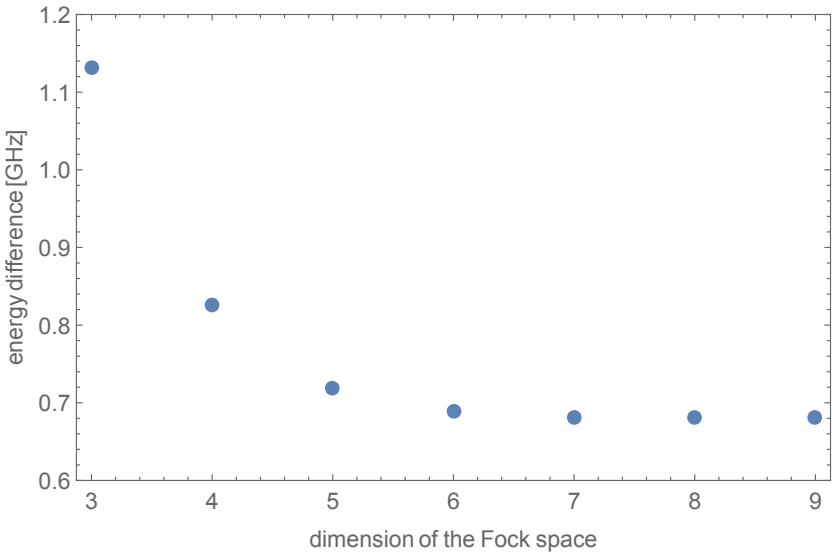

FIGURE 5.5: The dependence of the energy difference between the ground state $|g0\rangle \rightarrow |G\rangle$ and the first excited state $|e0\rangle \rightarrow |E\rangle_q$ on the dimension of the Fock space when $g = 0.1\omega_r$ and $f = 0.5$ with $\omega_r/2\pi = 10$ GHz and $\omega_{qb}/2\pi = 5$ GHz.

in the resonator, so that we truncate the parity chain at some point. This introduces an error and it is important to quantify the error before choosing the right number of the Fock states existing in the resonator field.

As we increase the coupling strength g, the system requires more Fock states to be properly truncated. A quick calculation shows that the error is about 0.0004 % between having three dimensional or four dimensional Fock space in the case of $g = 0.1\omega_r$, Fig. 5.3. So a three dimensional Fock space is sufficient for this specific case. Repeating the calculation for the case of $g = 0.5\omega_r$ gives 2.25 % error between three and four dimensional Fock spaces. The error decreases to 0.23 % between the four and five dimensional Fock spaces, which is more acceptable, Fig. 5.4. However, it is better to do the calculations with five Fock states existing in the resonator field, since the error between the four and five dimensions is 0.01 %, which is a desired threshold. Making calculations for the limit value, namely $g = \omega_r$, gives an error of 0.2 % between the seven and eight dimensional Fock spaces. Since the error is 0.033 between eight and nine dimensional Fock spaces, accepting the existence of eight Fock states in the field is acceptable though nine dimensional Fock space will lead to more precise results, Fig. 5.5.

By using the following parameters: $\Delta/2\pi = 5$ GHz, $\omega_r/2\pi = 10$ GHz and $f = 0.5$ so that $\omega_{qb} = \Delta$ with eight Fock states available in the resonator, we obtain the energy levels shown in Fig. 5.6. Inspecting energy values at $g = 0$ point helps us to label the states as $|g0\rangle, |e0\rangle, |g1\rangle, ...$, respectively from bottom to top. This plot also shows that the ground and first excited states approach which can also be found in literature,

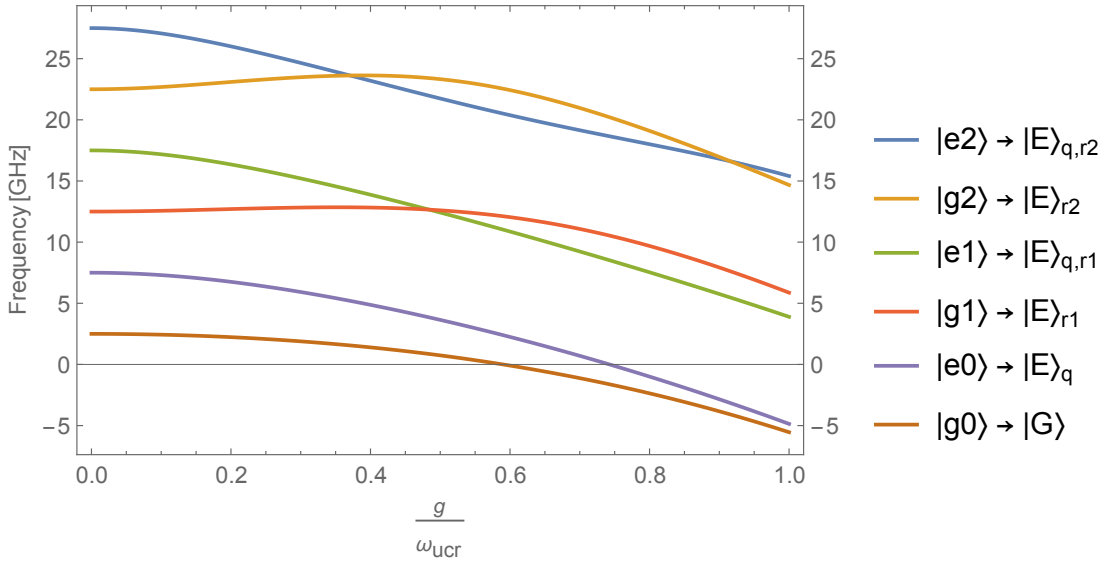

FIGURE 5.6: Energy levels of the quantum Rabi model with respect to g/ω_r using up to 11 Fock states in the resonator, at the symmetry point, $f = 0.5$ and $\omega_{qb} = 0.5\omega_r$.

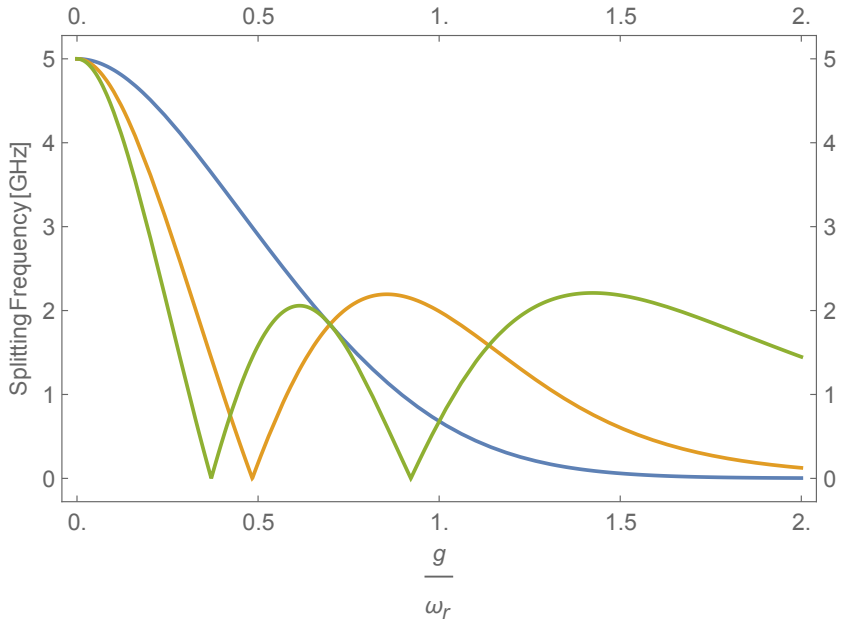

FIGURE 5.7: The spectrum of the quantum Rabi model with respect to g/ω_r using up to 11 Fock states in the resonator, at symmetry point $f = 0.5$ and $\omega_{qb} = 0.5\omega_r$. Blue line: $E_{|e0\rangle} - E_{|g0\rangle}$, orange line: $E_{|e1\rangle} - E_{|g1\rangle}$ and green line: $E_{|e3\rangle} - E_{|g3\rangle}$.

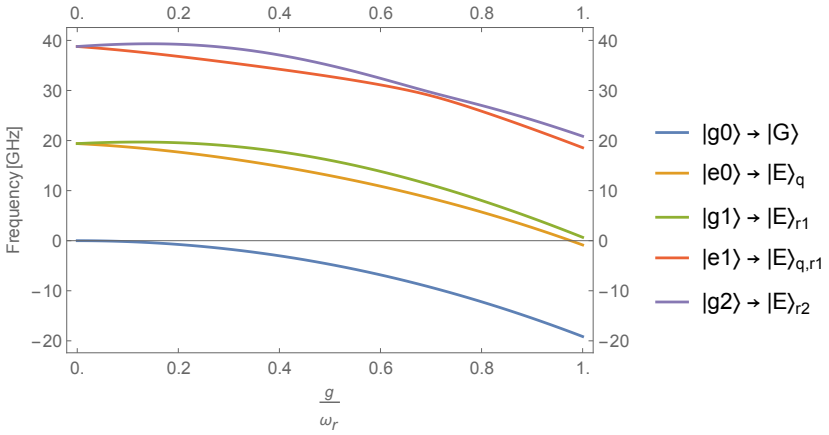

FIGURE 5.8: Energy levels of the quantum Rabi model with respect to g/ω_r using up to 8 Fock states in the resonator, at $f = 0.51$ and $\omega_{qb} = \omega_r$.

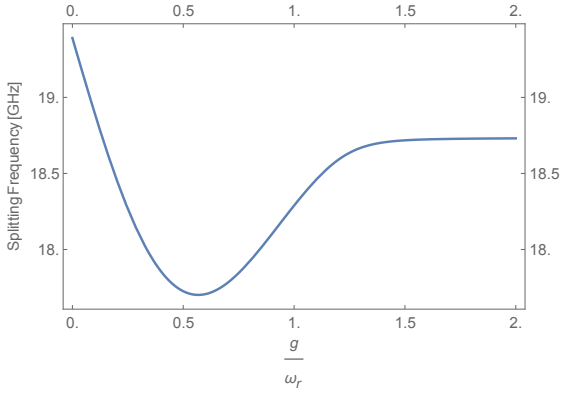

FIGURE 5.9: The energy difference $E_{|e0\rangle} - E_{|g0\rangle}$ of the quantum Rabi model with respect to g/ω_r using up to 8 Fock states in the resonator and at $f = 0.51$ and $\omega_{qb} = \omega_r$.

[1, 9]. One can additionally state that the ultrastrong coupling implies the existence of the bound photons in the resonator when the system is in the ground state due to the additional energy from the coupling [29]. This can be seen from the pairing of the lowest two energy levels in Fig. 5.6. As the coupling strength increases, pairs of states form between different parity chains and starting from around $g = 0.1\omega_r$ one cannot refer to the subsystems individually any more. These effects can be observed in Fig. 5.6 from the bending and crossings of the energy levels after $g = 0.1\omega_r$. The level-crossings seen in Rabi Model between different parity states at symmetry point are quite special and implies the symmetries that the system has, [9]. The energy differences, Fig. 5.7, show the expected behaviour of Laguerre polynomials [1] whose zeros represent the level-crossings in Fig. 5.6.

Lastly we will examine the case away from the symmetry point at $f = 0.51$, which results in a qubit frequency of $\omega_{qb}/2\pi = 19.4$ GHz (Fig. 5.8), meaning $\theta = \tan^{-1}(\epsilon/\Delta) = 75.1°$. As theory predicts [1], away from the symmetry point, the energy difference between the first excited state and the ground state, Fig. 5.9, converges to the magnetic energy ϵ

value, which is $\epsilon = 18.7$ GHz as the interaction becomes stronger. The reason behind this observation can be related to the domination of the coupling over the individual energies and since the coupling is through the magnetic field, the difference in the lowest two states converge to the magnetic energy value. The plot for the energy levels, Fig. 5.8, also shows similar behavior for the energy differences between excited levels. Furthermore, the energy levels do not cross as in the symmetric case and stay fixed to each other after some coupling strength, which is the expected behavior when the symmetry is broken in the quantum Rabi model, [9]. Therefore, it is reasonable to conclude that working away from the symmetry point blurs the effects observed in the ultrastrong regime.

The resulting system in ultrastrong coupling cannot be decomposed into a qubit and a resonator as in the Jaynes-Cummings model, which suggests a new integrated quantum system, with properties not experimentally observed yet [29].

Chapter 6

Readout Resonator Physics for Rabi Model

In current experiments using superconducting qubits, a readout resonator is used to measure the state of the qubit by placing the system in the dispersive regime [24]. Here we will propose adding a readout resonator weakly coupled to the qubit-resonator system that is in the ultrastrong coupling regime, as a way to extract the information from this novel and unknown quantum system. We first analyse the composition of the lowest four energy states as a function of qubit-resonator coupling strength. Our first main concern will be presenting a numerical proof of the disentanglement of the readout resonator from the rest of the system. This will allow us to probe the qubit-resonator system without affecting it. With this motivation we will investigate the energy level structure and the energy level shifts of the whole system numerically.

6.1 Description and Hamiltonian of the proposed model

From now on we will call the resonator which is ultrastrongly coupled to the qubit the ultrastrongly coupled resonator (UCR) and the new resonator the read-out resonator (RR). The RR will contribute to the Rabi Hamiltonian (5.2.2) with its own energy term and its coupling term to the UCR. The RR couples capacitively to the UCR. A schematic of the system is depicted in Fig. 6.1. It should be noted that the Rabi circuit and the readout resonator are excited with different signals in the same path, so that it is possible to excite the readout resonator with many photons by simultaneously restricting the number of photons to a small amount in the Rabi circuit.

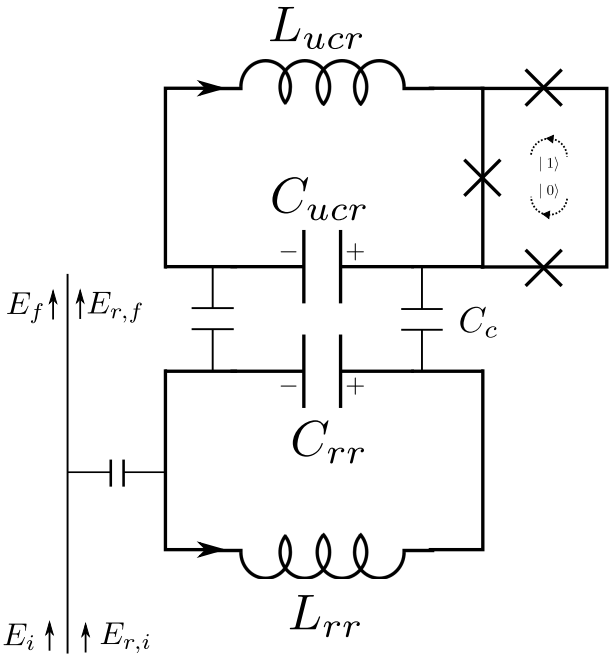

FIGURE 6.1: The circuit schematic of the proposed model to the analysis of Rabi Model.

Though it is quite straightforward to introduce the coupling term for two resonators, we will first study the case of two coupled harmonic oscillators classically. Then, we will quantize the system. Let us have different frequencies for the harmonic oscillators, ω_1 and ω_2, respectively. The coupling frequency will be ω_c. Then the Hamiltonian is:

$$H = \frac{p_1^2}{2m} + \frac{p_2^2}{2m} + \frac{1}{2}m\omega_1^2 x_1^2 + \frac{1}{2}m\omega_2^2 x_2^2 - m\omega_c^2 x_1 x_2. \tag{6.1.1}$$

If we apply Hamilton's equations, [26],

$$\frac{\partial H}{\partial p_\alpha} = \frac{dq_\alpha}{dt}, \tag{6.1.2}$$

$$\frac{\partial H}{\partial q_\alpha} = -\frac{dp_\alpha}{dt}, \tag{6.1.3}$$

we obtain the following coupled differential equations

$$\frac{d^2x_1}{dt^2} + \omega_1^2 x_1 - \omega_c^2 x_2 = 0, \tag{6.1.4}$$

$$\frac{d^2x_2}{dt^2} + \omega_2^2 x_2 - \omega_c^2 x_1 = 0. \tag{6.1.5}$$

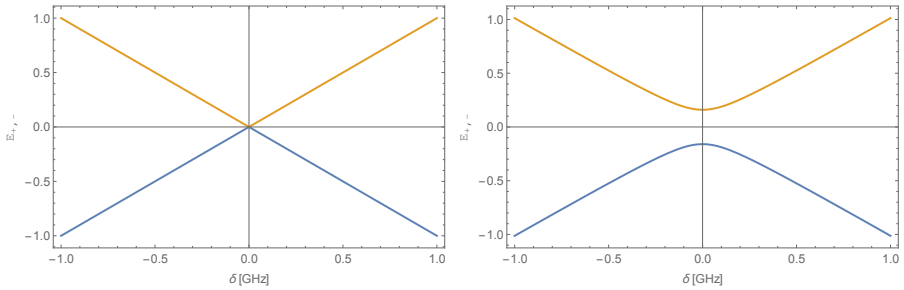

FIGURE 6.2: The classical energy splitting when two resonators are not coupled and coupled with a frequency of 0.4 GHz, respectively.

Assuming harmonic solutions, we substitute $\frac{d^2x_1}{dt^2} = -\omega_1^2 x_1$ and $\frac{d^2x_2}{dt^2} = -\omega_2^2 x_2$ in Eqs. (6.1.4) and (6.1.5),

$$\omega^2 \begin{pmatrix} x_1 \\ x_2 \end{pmatrix} = \begin{pmatrix} \omega_1^2 & -\omega_c^2 \\ \omega_c^2 & \omega_2^2 \end{pmatrix} \begin{pmatrix} x_1 \\ x_2 \end{pmatrix}. \tag{6.1.6}$$

Solving this eigenvalue problem leads us to,

$$\begin{aligned} \omega_{\mp}^2 &= \frac{\left(\omega_1^2 + \omega_2^2\right)}{2} \mp \sqrt{\left(\frac{\omega_1^2 + \omega_2^2}{2}\right)^2 - \left(\omega_1^2\omega_2^2 - \omega_c^4\right)}, \\ &= \frac{\left(\omega_1^2 + \omega_2^2\right)}{2} \mp \sqrt{\left(\frac{\omega_1^2 - \omega_2^2}{2}\right)^2 + \omega_c^4}. \end{aligned} \tag{6.1.7}$$

If we define a detuning parameter, $\delta = \frac{\omega_1^2 - \omega_2^2}{2}$ as the difference between the squares of the frequencies of the resonators, we can restate the eigenvalues:

$$\omega_{\mp}^2 = \frac{\left(\omega_1^2 + \omega_2^2\right)}{2} \mp \sqrt{\delta^2 + \omega_c^4}. \tag{6.1.8}$$

A plot for the eigenenergies with respect to the detuning when the coupling is zero and nonzero ($\omega_c = 0.4$ GHz) can be seen in Fig. 6.2, respectively. Since the current analysis is classical, it is interesting to observe an energy splitting which is similar to what we have found in Chapter 3 Fig. 3.1 for the eigenvalues of a general two-level system. Now in order to analyze the weak coupling regime for the two resonators, let us focus on the symmetry point, which implies $\delta = 0 \rightarrow \omega_1 = \omega_2 = \omega$. Rewrite eq. 6.1.8 for the symmetry point:

$$\omega_{\mp,s}^2 = \omega^2 \mp \omega_c^2. \tag{6.1.9}$$

where we assumed $\omega \gg \omega_c$ due to the weak coupling. Eigenvectors are $[1, 1]$ and $[1, -1]$. Then the solutions are generally:

$$x_{1,2}(t) = Ae^{i\omega_+ t} \pm Be^{i\omega_- t}. \tag{6.1.10}$$

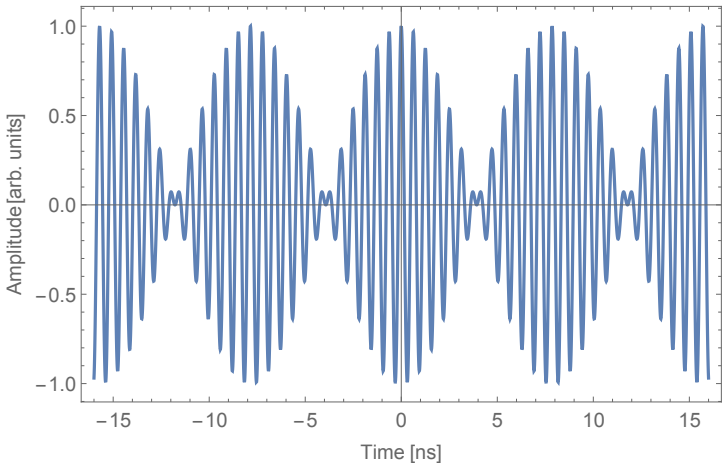

FIGURE 6.3: The beating phenomenon in the case of two coupled resonators of 10 GHz frequency at symmetry point, $\delta = 0$ with a coupling frequency of 0.4 GHz.

By using the appropriate initial conditions, one can end up with the following:

$$x_{1,2}(t) = \frac{A}{2}\left(\cos\omega_+ t \pm \cos\omega_- t\right), \tag{6.1.11}$$

which can also be written as

$$x_1(t) = A\cos\left(\frac{\omega_+ + \omega_-}{2}t\right)\cos\left(\frac{\omega_+ - \omega_-}{2}t\right), \tag{6.1.12}$$

$$x_2(t) = A\sin\left(\frac{\omega_+ + \omega_-}{2}t\right)\sin\left(\frac{\omega_+ - \omega_-}{2}t\right). \tag{6.1.13}$$

which exhibit the beating phenomenon, [26]. A plot for Eq. 6.1.12 can be seen in Fig. 6.3.

Now let us quantize the coupled harmonic oscillators, by turning classical variables into quantum operators obeying commutation relations $[\hat{p}_i, \hat{x}_j] = i\hbar\delta_{ij}$, as also performed in the quantization of the free electromagnetic field.

$$\hat{H} = \frac{\hat{p}_1^2}{2m} + \frac{\hat{p}_2^2}{2m} + \frac{1}{2}m\omega_1^2\hat{x}_1^2 + \frac{1}{2}m\omega_2\hat{x}_2^2 - m\omega_c^2\hat{x}_1\hat{x}_2. \tag{6.1.14}$$

By expressing the momentum $\hat{p}$ and position $\hat{x}$ operators in terms of annihilation and creation operators $\left\{\hat{a}, \hat{a}^\dagger\right\}$ [5],

$$\hat{x} = \sqrt{\frac{\hbar}{2m\omega}}\left(\hat{a}^\dagger + \hat{a}\right), \tag{6.1.15}$$

$$\hat{p} = i\sqrt{\frac{\hbar m\omega}{2}}\left(\hat{a}^\dagger - \hat{a}\right). \tag{6.1.16}$$

Let us denote the annihilation operator of the first oscillator as $\hat{a}$ and the second one as $\hat{b}$. Then the Hamiltonian for the two coupled oscillators is,

$$\hat{H} = \hbar\omega_1 \left(\hat{a}^\dagger \hat{a} + \frac{1}{2}\right) + \hbar\omega_2 \left(\hat{b}^\dagger \hat{b} + \frac{1}{2}\right) - \frac{\hbar\omega_c^2}{2\sqrt{\omega_1\omega_2}} \left(\hat{a}^\dagger + \hat{a}\right)\left(\hat{b}^\dagger + \hat{b}\right). \tag{6.1.17}$$

Let us now add these additional terms to the Rabi Hamiltonian (5.2.1):

$$\begin{aligned}\hat{H} = {} & \frac{\hbar\Delta}{2}\sigma_x + I_p\Phi_o \left(f - \frac{1}{2}\right)\sigma_z + \hbar g\sigma_z(\hat{a} + \hat{a}^\dagger) + \hbar\omega_{UCR}\left(\hat{a}^\dagger\hat{a} + \frac{1}{2}\right) \\ & + \hbar\omega_{RR}\left(\hat{b}^\dagger\hat{b} + \frac{1}{2}\right) - \hbar g_r \left(\hat{a}^\dagger + \hat{a}\right)\left(\hat{b}^\dagger + \hat{b}\right),\end{aligned} \tag{6.1.18}$$

where $g_r = \frac{\omega_c^2\hbar}{2\sqrt{\omega_{UCR}\omega_{RR}}}$. We will solve the Hamiltonian (6.1.18) with different parameters throughout the following sections. The first set of parameters is $\Delta/2\pi = 5$ GHz, $\omega_{UCR}/2\pi = 10$ GHz, $\omega_{RR}/2\pi = 9$ GHz, $\omega_c/2\pi = 1$ GHz so that the total coupling between the resonators is $g_r = 52.7$ MHz. This set has a large detuning between the qubit and the ultrastrongly coupled resonator. The second set of parameters is $\Delta/2\pi = 12$ GHz, $\omega_{UCR}/2\pi = 10$ GHz, $\omega_{RR}/2\pi = 9$ GHz and $\omega_c/2\pi = 1$ GHz, which results the same g_r coupling between the resonators. The third set of parameters is $\Delta/2\pi = 9.5$ GHz, $\omega_{UCR}/2\pi = 10$ GHz, $\omega_{RR}/2\pi = 9$ GHz and $\omega_c/2\pi = 1$ GHz. The last set represents a small amount of detuning of the qubit with both the RR and UCR. The parameters regarding the flux qubit are same as in Rabi and JC models.

6.2 Energy shift analysis in a readout resonator for Jaynes-Cummings model

Before starting the analysis, in order to show how the RR reads the information in the UCR-qubit system, we will make use of the dispersive regime analysed in Chapter 4. Restating the JC Hamiltonian 4.3.4 in dispersive regime,

$$H_{JC}^d \approx \hbar\left(\omega_{RR} + \frac{g_r^2}{\delta}\sigma_z\right)a^\dagger a + \frac{\hbar}{2}\left(\omega_{qb} + \frac{g^2}{\delta}\right)\sigma_z, \tag{6.2.1}$$

with $\sin\theta = 1$ because of the symmetry point, we can calculate the approximate initial energy shift at $g = 0$, since g_r is weakly coupled to the system. Even though Eq. (6.2.1) is not exactly the formulation for the current problem, it is useful to make this analysis to show the readout process. By using Eq. (6.2.1),

$$E_{|g0\rangle} = -\frac{\hbar}{2}\left(\omega_{qb} + \frac{g_r^2}{\delta}\right) + E_{zpe} \tag{6.2.2}$$

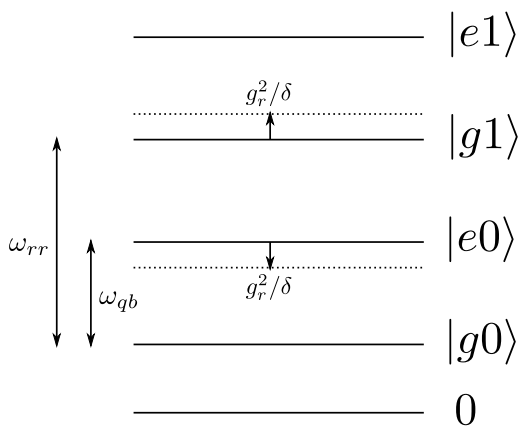

FIGURE 6.4: The schematic which shows the energy shifts in dispersive regime.

$$E_{|e0\rangle} = \frac{\hbar}{2}\left(\omega_{qb} + \frac{g_r^2}{\delta}\right) + E_{zpe} \tag{6.2.3}$$

$$E_{|g1\rangle} = \hbar\left(\omega_{RR} - \frac{g_r^2}{\delta}\right) - \frac{\hbar}{2}\left(\omega_{qb} + \frac{g_r^2}{\delta}\right) + E_{zpe} \tag{6.2.4}$$

$$E_{|e1\rangle} = \hbar\left(\omega_{RR} + \frac{g_r^2}{\delta}\right) + \frac{\hbar}{2}\left(\omega_{qb} + \frac{g_r^2}{\delta}\right) + E_{zpe} \tag{6.2.5}$$

Subtracting $E_{|g1\rangle} - E_{|g0\rangle} = \hbar\omega_{RR} - \hbar\frac{g_r^2}{\delta}$ gives the formulation for the qubit in the ground state and for the qubit excited state, $E_{|e1\rangle} - E_{|e0\rangle} = \hbar\omega_{RR} + \hbar\frac{g_r^2}{\delta}$, which can also be seen in Fig. 6.4. So, we can conclude that when the qubit is in its ground state, the energy shift observed in the readout resonator will be $-\frac{g_r^2}{\delta}$ and when the qubit is in its excited state, the energy shift in the RR will be $\frac{g_r^2}{\delta}$. Therefore, we would measure the state of the qubit without affecting it, a process called *quantum nondemolition measurement* .

In our system, the readout resonator is weakly coupled to the UCR. So we can expect a similar behaviour in the energy shift for the two weakly coupled resonators with the difference factor of $\frac{g_r^2}{\delta}$, where where $g_r = \frac{\omega_c^2}{2\sqrt{\omega_{UCR}\omega_{RR}}}$ and $\delta = \omega_{UCR} - \omega_{RR}$. If we use the parameters defined at the beginning of the chapter, we obtain $\frac{g_r^2}{\delta} = 2.78$ MHz.

6.3 Analysis of the system with first set of parameters

We will first determine the compositions of the lowest four states and the amount of the entanglement of RR with the rest of the system to show that the first set of parameters are useful to work with. Then we will investigate the energy level structure and the energy shifts between specific levels.

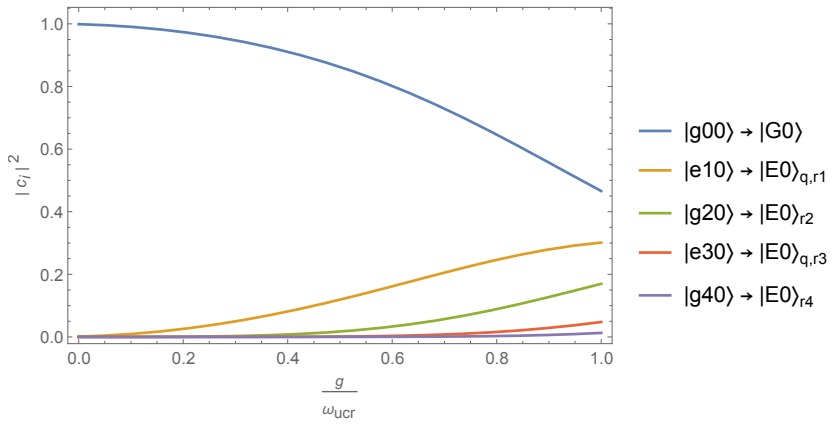

FIGURE 6.5: The decomposition of the state $|G0\rangle$ to the other states with respect to g coupling.

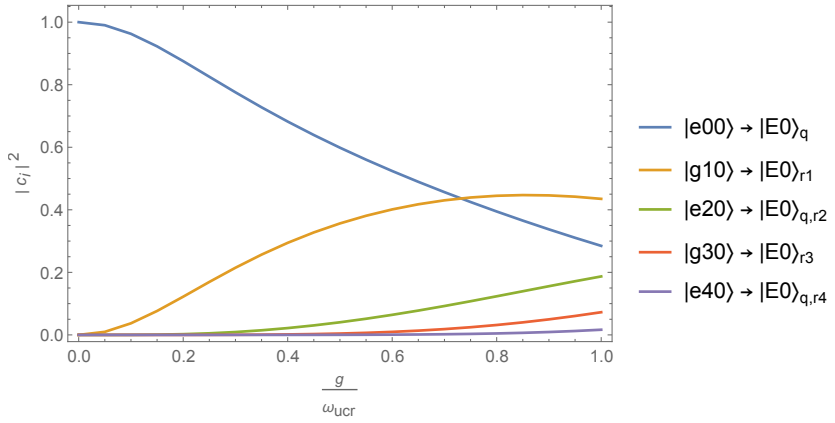

FIGURE 6.6: The decomposition of the state $|E0\rangle_q$ to the other states with respect to g coupling.

6.3.1 Composition of the states with respect to the coupling strength

We focused here on the composition of the four lowest energy states. By inspecting the energy levels with $g = 0$ coupling, we find that the order of first four lowest states $|g00\rangle, |e00\rangle, |g01\rangle, |g10\rangle$.

The ground state of the coupled system will be in general,

$$|\phi\rangle = \sum_i c_i |\psi_i\rangle , \tag{6.3.1}$$

where $|g00\rangle$ is denoted as $|G0\rangle$ for an arbitrary value of the coupling strength between the qubit and UCR. $|\psi_i\rangle$ is an arbitrary state of the coupled system and c_i is the associated weight coefficient. As observed in Fig. 6.5, the ground state $|G0\rangle$ decomposes into a superposition of $|E0\rangle_{q,r1}$, $|E0\rangle_{r2}$, $|E0\rangle_{q,r3}$ and $|E0\rangle_{r4}$ as the coupling strength increases. Such a decomposition represents the excitation dynamics at $p = 1$ parity chain in Hilbert space. Similarly for the first excited state of the coupled system $|E0\rangle_q$ which is the state

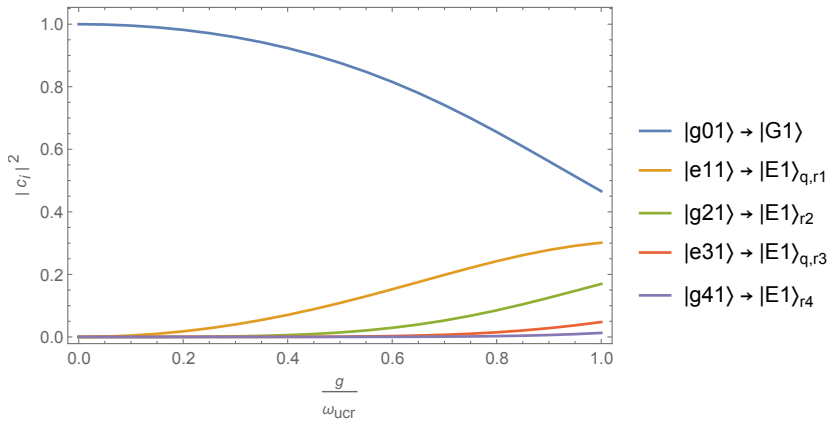

FIGURE 6.7: The decomposition of the state $|G1\rangle$ to the other states with respect to g coupling.

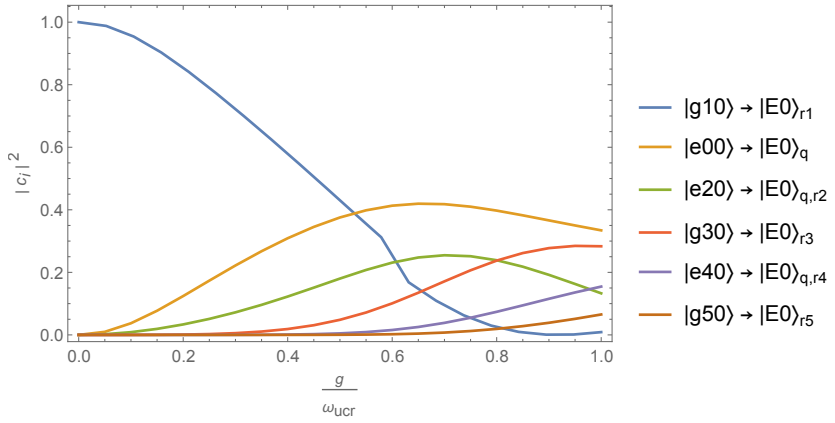

FIGURE 6.8: The decomposition of the state $|E0\rangle_{r1}$ to the other states with respect to g coupling.

where the qubit is excited, $|\psi_i\rangle$ will be $|E0\rangle_{r1}$, $|E0\rangle_{q,r2}$, $|E0\rangle_{r3}$ and $|e40\rangle_{q,r4}$, Fig. 6.6. This decomposition represents the photon dynamics at the negative, $p = -1$ parity chain in Hilbert space. The state where only the RR is excited with a single excitation, $|G1\rangle$ mainly decomposes into the states in the positive parity chain with a single excitation in RR, Fig. 6.7. Lastly, Fig. 6.8 shows the decomposition of the state where only UCR is excited with a single excitation, $|E0\rangle_{r1}$ which decomposes into states in both directions in the negative parity chain.

6.3.2 The amount of the entanglement between RR and the Rabi system

Even though the compositions of the lowest four states mainly contain the states in their associated parity chains, because of the weak coupling between the resonators there is a small but finite amount of probability that the RR states are entangled to the rest of the system. Fig. 6.9 shows the possible state transitions in the qubit-UCR-RR system. The

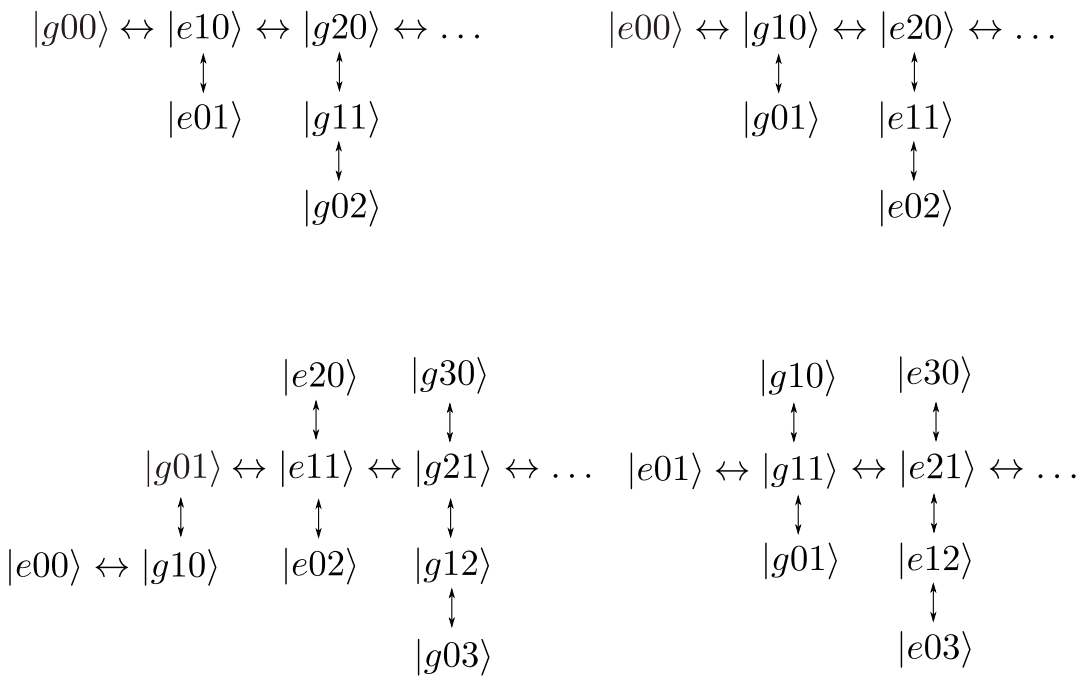

FIGURE 6.9: The horizontal chains show the excitations taking place inside the parity chains of Quantum Rabi model both with rotating and counter-rotating terms. The vertical chains show the excitations between the resonators with only rotating terms.

horizontal chains are the parity chains of the Quantum Rabi Model, while the vertical chains show the resonator-resonator interactions.

The probabilities, $|c_i|^2$, of the entanglement between the RR and the rest of the system at the coupling strength $g = \omega_{ucr}$ are shown in Tables 6.1, 6.2 and 6.3. Let us also emphasize that when $|\psi_i\rangle = |G1\rangle$ in the decomposition of the state $|G0\rangle$, $|c_i|^2 \propto 10^{-32}$ and similarly in the decomposition of $|G1\rangle$, when $|\psi_i\rangle = |G0\rangle$, $|c_i|^2 \propto 10^{-30}$. Therefore, for the first set of parameters, we can conclude that the RR is not coupled to the UCR-qubit system strongly enough to create an excitation in RR. So, for a detuning of $\omega_{qb} = 0.5\omega_{ucr}$, we can write $|\psi_{sys}\rangle = |UCR - qb\rangle\,|RR\rangle$ and analyze the energy shifts.

Decomposed state	$\|e01\rangle$	$\|g02\rangle$	$\|g11\rangle$	$\|g01\rangle$	$\|e02\rangle$	$\|e11\rangle$
$\|g00\rangle$	1.089×10^{-3}	2.25×10^{-6}	1.225×10^{-3}	0	0	0
$\|e00\rangle$	0	0	0	1.6×10^{-3}	2.56×10^{-6}	1.369×10^{-3}
$\|e10\rangle$	9.6×10^{-3}	10^{-4}	0.02	0	0	0

TABLE 6.1: The table for the decomposition of $|g00\rangle$, $|e00\rangle$ and $|e10\rangle$ in terms of sub-chain states.

Decomposed state	$\|g10\rangle$	$\|e00\rangle$	$\|e02\rangle$	$\|e20\rangle$	$\|g01\rangle$	$\|e11\rangle$
$\|g01\rangle$	1.849×10^{-3}	2.25×10^{-4}	2.116×10^{-3}	1.444×10^{-3}	PC	PC
$\|g10\rangle$	PC	PC	10^{-8}	PC	5.76×10^{-4}	3.24×10^{-4}

TABLE 6.2: The table for the decomposition of $|g01\rangle$ and $|g10\rangle$ in terms of sub-chain states. PC stands for parity chain.

Decomposed state	$\|e10\rangle$	$\|g00\rangle$	$\|g02\rangle$	$\|g20\rangle$
$\|g11\rangle$	0.03	0.01	9×10^{-4}	0.015
$\|e01\rangle$	4.225×10^{-3}	6.4×10^{-3}	3.36×10^{-3}	0.0196

TABLE 6.3: The table for the decomposition of $|g11\rangle$ and $|e01\rangle$ in terms of sub-chain states.

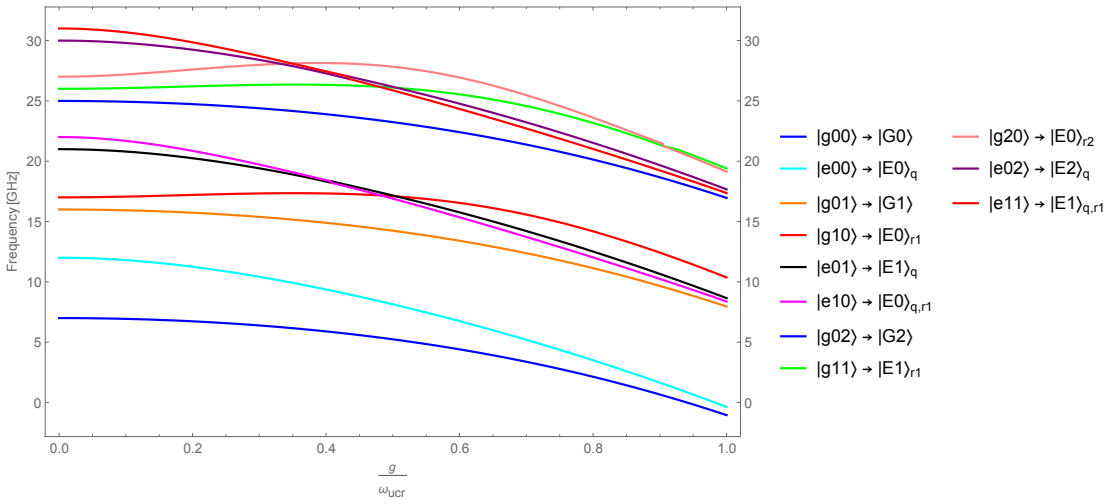

FIGURE 6.10: The energy levels of qubit-UCR-RR system at symmetry point, $f = 0.5$ with respect to g/ω_{UCR}.

6.3.3 Energy level structure and energy shifts

Since we are working at the symmetry point, the level-crossings of the energy levels can be observed in the case of fast transition between different parity chains, Fig. 6.10. Similar to Rabi energy level plots in Chapter 5, the first excited state approaches to the ground state. Fig. 6.11 shows the energy level structure of only qubit-UCR states, $|UCR - qb\rangle$, which is quite similar to the Rabi model plot, Fig. 5.6, except the zero point energies which are different due to the extra resonator introduced to the system. So, this also shows that the RR states might be separable from the qubit-UCR states, which is an observation that has been shown in the previous sections.

We then inspected the energy shifts between the states with only one excitation and no excitation in RR as the coupling strength g_{UCR-qb} increases. Different energy shifts are

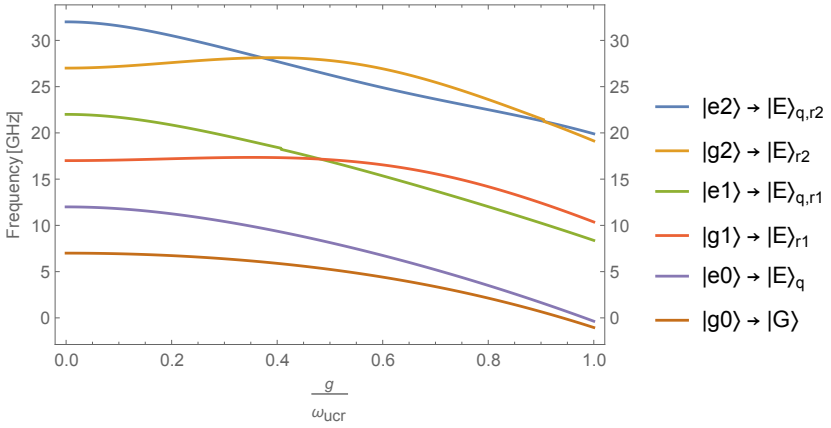

FIGURE 6.11: The energy levels of only qubit-UCR states of qubit-UCR-RR system at symmetry point, $f = 0.5$ with respect to g/ω_{UCR}.

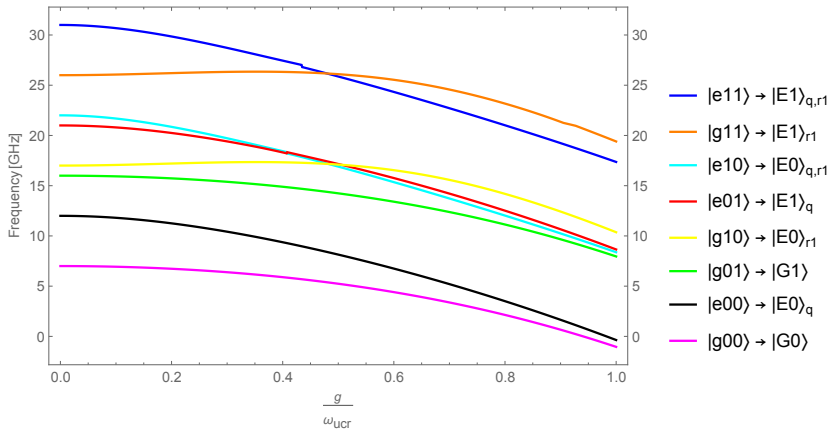

FIGURE 6.12: The energy levels of only the states of energy shifts at symmetry point, $f = 0.5$ with respect to g/ω_{UCR}.

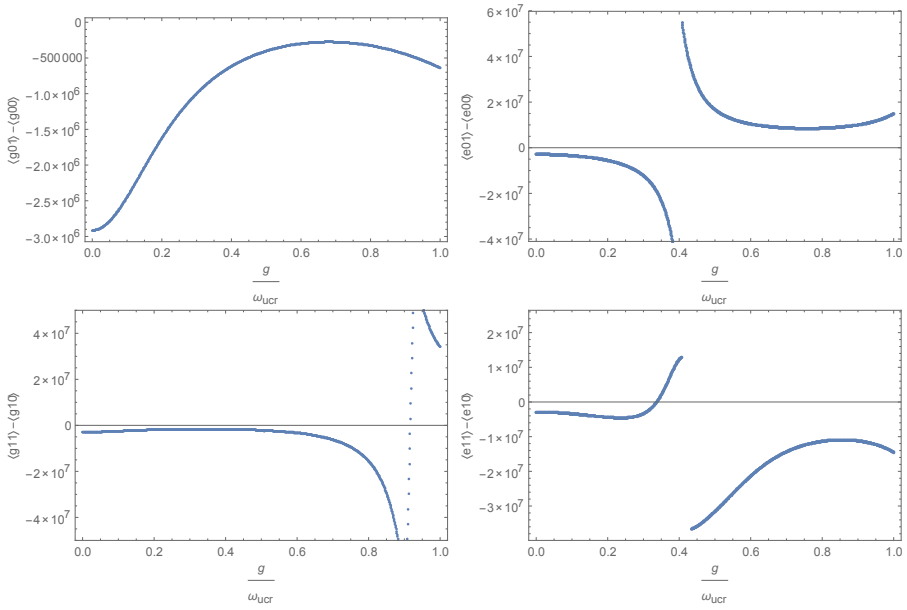

FIGURE 6.13: The energy shift between $\langle g01\rangle - \langle g00\rangle$, $\langle e01\rangle - \langle e00\rangle$, $\langle g11\rangle - \langle g10\rangle$ and $\langle e11\rangle - \langle e10\rangle$, respectively.

expected in ω_{RR} for the qubit ground and excited states in order to differentiate the two.

The energy level structure for only the states with shifts is given in Fig. 6.12. It can be observed that all of the energy shifts start at 2.91 MHz at $g = 0$, which is quite close to the calculated value, 2.78 MHz in Section 6.2. The plots in Fig. 6.13 shows the energy shifts between $\langle g01\rangle$ and $\langle g00\rangle$, $\langle e01\rangle$ and $\langle e00\rangle$, $\langle g11\rangle$ and $\langle g10\rangle$, $\langle e11\rangle$ and $\langle e10\rangle$, respectively. Energy shifts have discontinuous parts, which is originated due to the level-crossings, which is irrelevant to the problem we are interested.

The energy shifts for the ground state of the system, $\langle g01\rangle - \langle g00\rangle$, and the first excited

state of the system, $\langle e01\rangle - \langle e00\rangle$ are different enough to differentiate the two. In the interval of $g = 0 - 0.4$, $\langle g01\rangle - \langle g00\rangle$ increases while $\langle e01\rangle - \langle e00\rangle$ decreases, which leads to different amount of energy shifts for them. Starting from $g = 0.5$ until the end, $\langle e01\rangle - \langle e00\rangle$ changes its sign and becomes stabilized around 10 MHz, which is again sufficiently different than the energy shift of the $\langle g01\rangle - \langle g00\rangle$.

The energy shift for $\langle g11\rangle - \langle g10\rangle$ behaves similar to $\langle g01\rangle - \langle g00\rangle$ except very high couplings. Because of the discontinuity in the energy shift plot of $\langle g11\rangle - \langle g10\rangle$, it is hard to obtain a value and compare with the other shifts for the high coupling strengths. For the interval $g = 0 - 0.3$, the shift $\langle e11\rangle - \langle e10\rangle$ decreases in contrast to the increase in the energy shift of the ground state. Lastly, for the interval $g = 0.5 - 1$, this energy shift is around -10 MHz, while the energy shift for the ground state is around -0.5 MHz, which makes the state $|e10\rangle$ indistinguishable from the ground state, as well.

6.4 Analysis of the system with the second set of parameters

The second set of parameters are $\Delta/2\pi = 12$ GHz, $\omega_{UCR}/2\pi = 10$ GHz, $\omega_{RR}/2\pi = 9$ GHz, $\omega_c/2\pi = 1$ GHz so that the detuning is 2 GHz. In this section, we will repeat the whole procedure which are performed for the first set of parameters on the second set of parameters.

6.4.1 Composition of the states with respect to coupling strength

By inspecting the energy levels with $g = 0$ coupling, we find that the order of first four lowest states $|g00\rangle, |g01\rangle, |g10\rangle, |e00\rangle$.

Similar to the first set of parameters, the states of the coupled system will be in general,

$$|\phi\rangle = \sum_i c_i |\psi_i\rangle . \tag{6.4.1}$$

As observed in Fig. 6.14, the ground state $|G0\rangle$ decomposes into a superposition of $|E0\rangle_{q,r1}$, $|E0\rangle_{r2}$ and $|E0\rangle_{q,r3}$ mostly as the coupling strength increases. Such a decomposition represents the excitation dynamics at $p = 1$ parity chain in Hilbert space. Similarly for an excited state of the coupled system $|E0\rangle_q$ which is the state where the qubit is excited, $|\psi_i\rangle$ will be $|g10\rangle$, $|e20\rangle, |g30\rangle$, $|e40\rangle$ and $|g50\rangle$, Fig. 6.15. This decomposition represents the photon dynamics at the negative, $p = -1$ parity chain in Hilbert space. The state where only the RR is excited with a single excitation, $|G1\rangle$ mainly

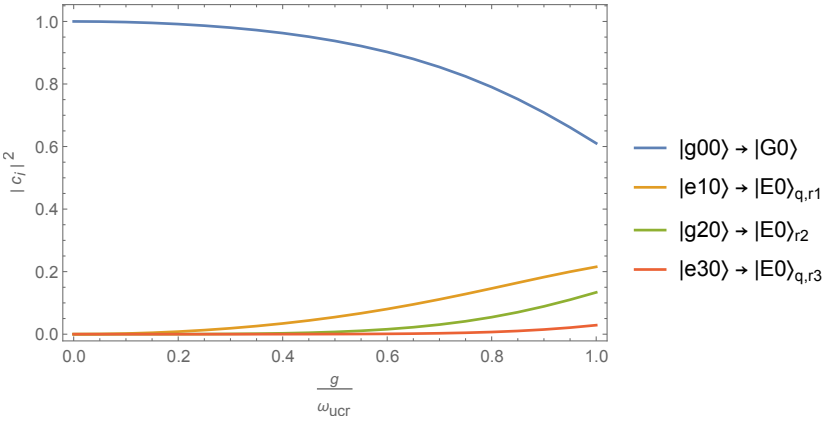

FIGURE 6.14: The decomposition of the state $|G0\rangle$ to the other states with respect to g coupling.

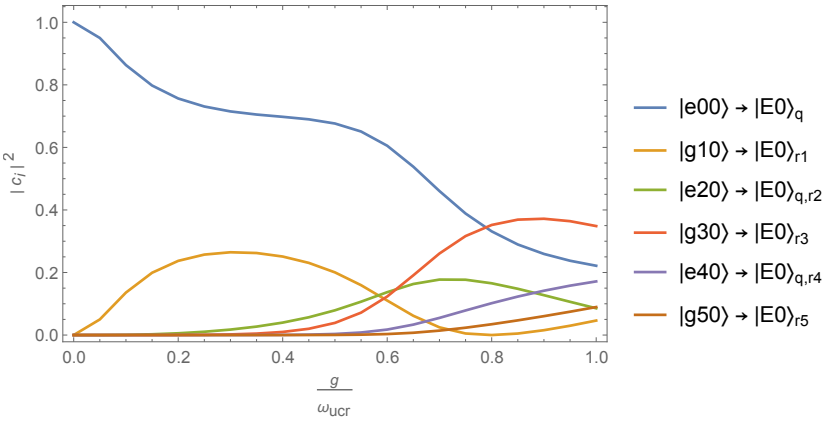

FIGURE 6.15: The decomposition of the state $|E0\rangle_q$ to the other states with respect to g coupling.

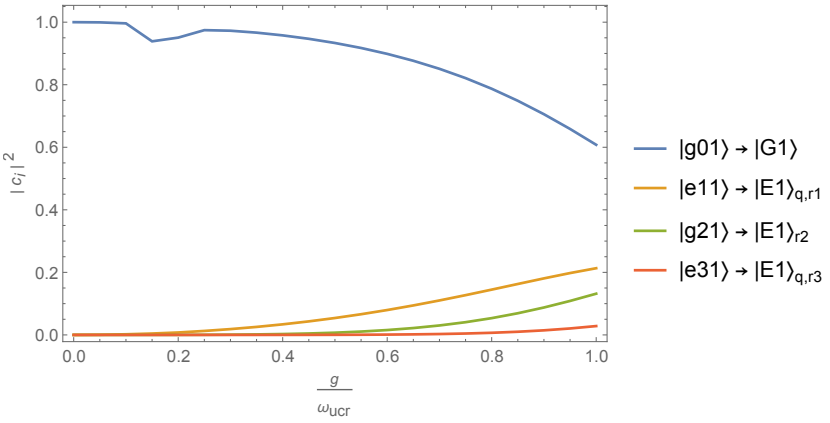

FIGURE 6.16: The decomposition of the state $|G1\rangle$ to the other states with respect to g coupling.

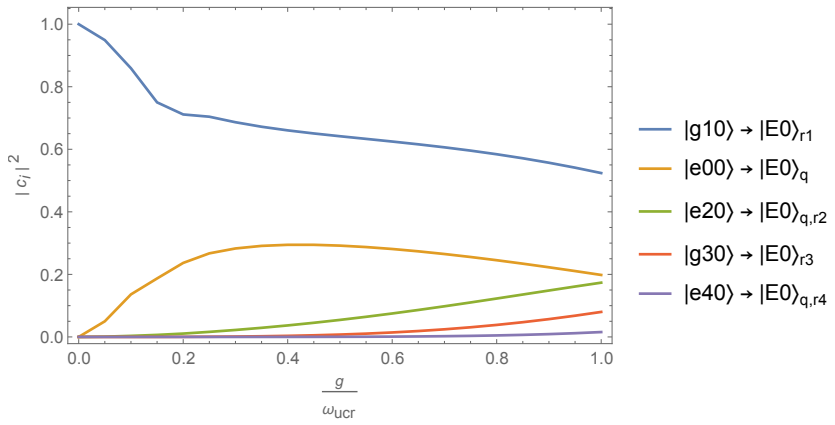

FIGURE 6.17: The decomposition of the state $|E0\rangle_{r1}$ to the other states with respect to g coupling.

decomposes into the states in the positive parity chain with a single excitation in RR, Fig. 6.16. Lastly, Fig. 6.17 shows the decomposition of the state where only UCR is excited with a single excitation, $|E0\rangle_{r1}$ which decomposes into states in both directions in the negative parity chain.

The decomposition of the state $|E0\rangle_q$, Fig. 6.15, has some other interesting features. When the coupling is weaker than $g = \omega_{ucr,qb}$, $|E0\rangle_q$ mostly decomposes into the state $|E0\rangle_{r1}$ which is the only possible state transition in Jaynes-Cummings model. However as the coupling strength increases, other states in the negative parity chain of Rabi model are more preferred to decompose. A similar effect can also be observed in the decomposition of the state $|E0\rangle_{r1}$, which mostly decomposes into the state $|E0\rangle_q$ in the interval of $g = 0 - 0.2$ and then prefers to decompose more into the other states in the negative parity chain, Fig. 6.17. This behavior can also be observed for the first set of parameters in Figs. 6.6-6.8, though not as obvious as in the second set of parameters. Such a difference might be interpreted as the effect of detuning between the qubit and UCR frequencies.

These decomposition plots indicate a coupling between the RR and the rest of the system weak enough to assume that the wavefunction of the RR might in fact be separable from the wavefunction of the Rabi model. A quick analysis also shows that the probability, $|c_i|^2$ of $|\psi_i\rangle = |G1\rangle$ in the decomposition of the state $|G0\rangle$ is around $\propto 10^{-32}$. Similarly, in the decomposition of $|G1\rangle$, when $|\psi_i\rangle = |G0\rangle$, $|c_i|^2 \propto 10^{-32}$. Similar to the analysis with the first set of parameters, the states in this section also experience the resonator-resonator interactions and decompose into the states in the vertical chains in Fig. 6.9.

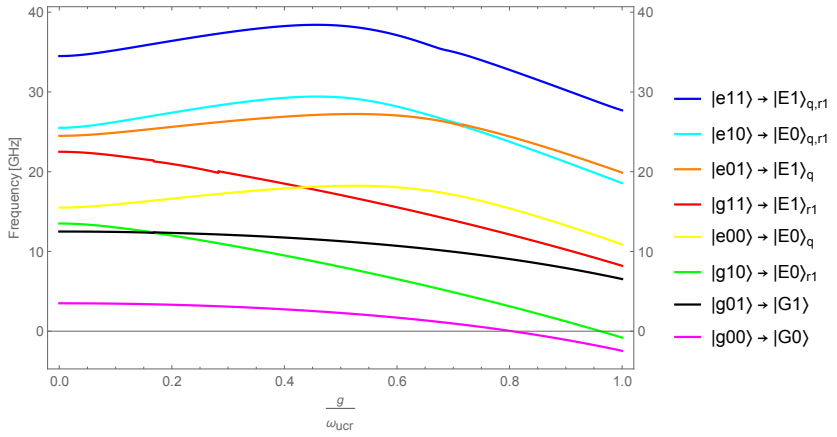

FIGURE 6.18: The energy levels of only the states of energy shifts at symmetry point, $f = 0.5$ with respect to g/ω_{UCR} with the second set of parameters.

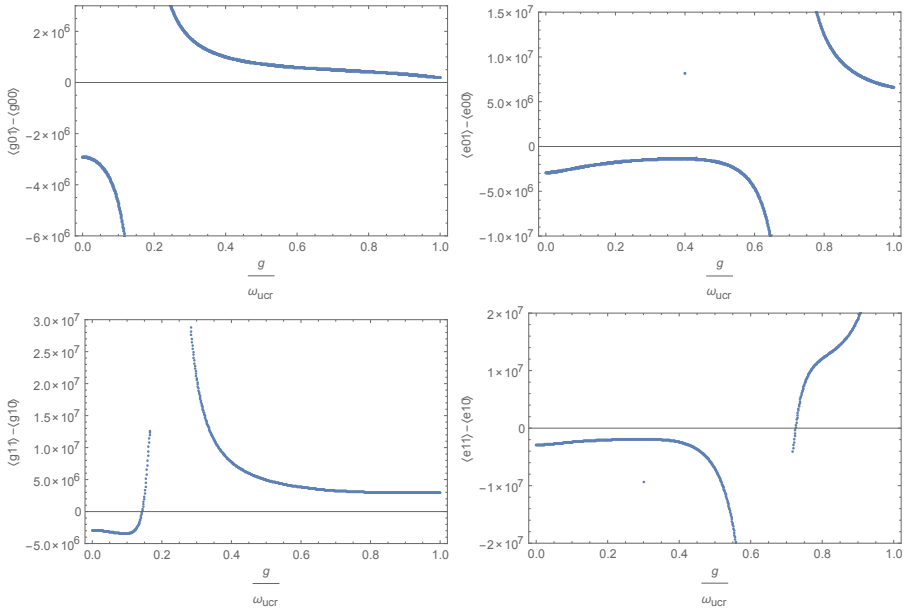

FIGURE 6.19: The energy shift between $\langle g01\rangle - \langle g00\rangle$, $\langle e01\rangle - \langle e00\rangle$, $\langle g11\rangle - \langle g10\rangle$ and $\langle e11\rangle - \langle e10\rangle$, respectively with the second set of parameters.

6.4.2 Energy level structure and the energy shifts

The energy level structure for the second set of parameters can be seen in Fig. 6.18. Only the required states for the energy shifts are depicted. Similar to the first set of parameters, all the energy shifts for the detuning of 2 GHz start from 2.91 MHz at $g = 0$. Energy shifts for $\langle g01\rangle - \langle g00\rangle$, $\langle e01\rangle - \langle e00\rangle$, $\langle g11\rangle - \langle g10\rangle$ and $\langle e11\rangle - \langle e10\rangle$ can be seen in Fig. 6.19, respectively.

Since the first excited state is $|g10\rangle$ for most of the coupling values, Fig. 6.18, let us compare the energy shifts for $\langle g01\rangle - \langle g00\rangle$ and $\langle g11\rangle - \langle g10\rangle$ starting from $g = 0.2$ until the end. Interestingly these two plots behave quite much the same, though the amount

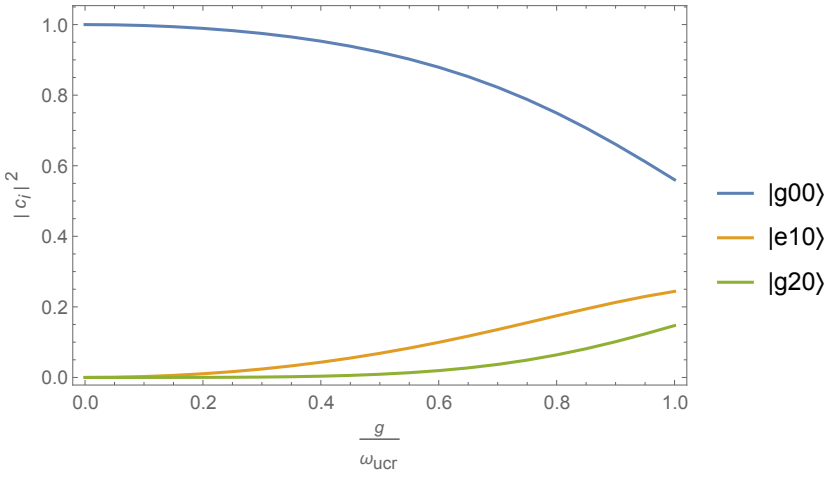

FIGURE 6.20: The decomposition of the state $|g00\rangle$ to the other states with respect to g coupling.

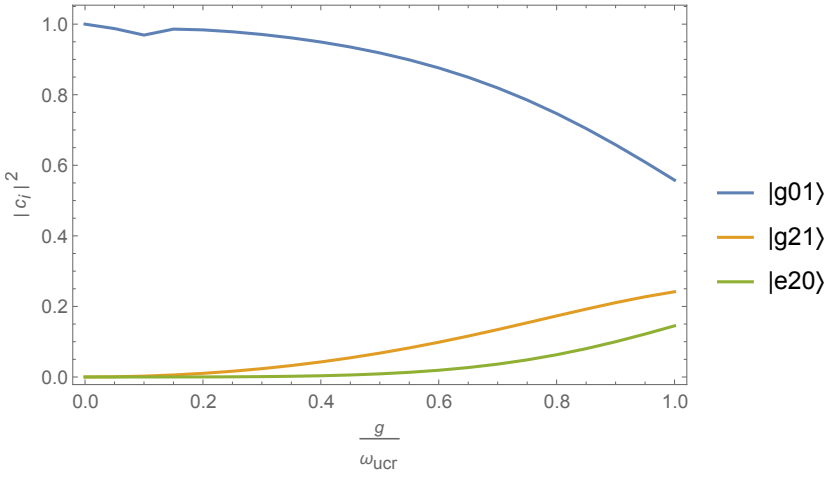

FIGURE 6.21: The decomposition of the state $|g01\rangle$ to the other states with respect to g coupling.

of their energy shifts are different, which is required for the states to be distinguishable. The amounts of the energy shifts for $\langle e01\rangle - \langle e00\rangle$ and $\langle e11\rangle - \langle e10\rangle$ are almost the same ($\approx$ 10 GHz) in the interval of $g = 0 - 0.6$ and that makes the states $|e00\rangle$ and $|e10\rangle$ indistinguishable from the ground state.

6.5 Analysis of the system with the third set of parameters

The third set of parameters are $\Delta/2\pi = 9.5$ GHz, $\omega_{UCR}/2\pi = 10$ GHz, $\omega_{RR}/2\pi = 9$ GHz, $\omega_c/2\pi = 1$ GHz so that the detuning is 0.5 GHz. We will show that for the third set of parameters, the readout resonator is not sufficiently decoupled from the rest of the system, so that this set of parameters is not an ideal set of parameters.

As observed in Fig. 6.20, the ground state $|g00\rangle$ decomposes into a superposition of the states in the positive parity chain as the coupling strength increases and show a sufficient decoupling from the RR states. However, the first excited state of the coupled system, $|g01\rangle$ couples more to the state $|e20\rangle$ via bypassing $|e11\rangle$ which is a state also in the positive parity chain with an excitation in the RR. Fig. 6.21 shows that the readout resonator is entangled to the rest of the system so that the whole wavefunction of the system cannot be decomposed. Therefore, the third set of parameters is not an ideal set of parameters to read-out the state of the system in a QND experiment.

Chapter 7

Conclusions

In this thesis, we first quantized the free electromagnetic field, LC resonator and the 1D transmission line. Then we introduced the Hamiltonian for the flux qubit under constant and time-dependent magnetic fields as a model for two-level system. We analysed the combined light-matter interaction system of the flux qubit and the resonator as Jaynes-Cummings model, deriving the dressed states for the model when the coupling strength is non-zero. We then applied the ultra-strong coupling regime to the flux qubit-resonator system, which required $g \approx \omega_{qb,r}$. We showed that it is not possible to discuss about the individual subsystems in the ultrastrong coupling regime and the whole system becomes a single integrated quantum system, which behaves quite distinct from the predictions of the Jaynes-Cummings model. Therefore, we proposed a quantum nondemolition (QND) measurement system to readout the information stored in this unknown quantum system, namely adding a readout resonator to the system.

We then showed that the readout resonator is in fact separable than the rest of the system, when the coupling strength between the resonators is much smaller than the ultrastrongly coupled resonator and the qubit for 5 GHz and 2 GHz detunings. This made us probe to the system without affecting the states of the system. We first generated the decomposition plots of the lowest four states, which turned out to be consistent with the intuitive mental picture of *parity state chains* of Quantum Rabi Model. Then we showed the energy level structure of the system and the weak entanglement between the readout resonator and the rest of the system, which make the readout resonator separable from the rest of the system. Then we calculated the energy shifts with respect to the coupling strength. Different amounts of energy shifts are observed for the ground and first excited states, which is a conclusion that shows the proposed QND mechanism is possible to construct for the experimental observation of the states of this quantum

object. An analytic expression for the energy shifts is aimed to be derived for further research.

Bibliography

[1] S. Ashhab and Franco Nori. Qubit-oscillator systems in the ultrastrong-coupling regime and their potential for preparing nonclassical states. *Phys. Rev. A*, 81: 042311, Apr 2010. doi: 10.1103/PhysRevA.81.042311. URL http://link.aps.org/doi/10.1103/PhysRevA.81.042311.

[2] M. Planck. On the theory of the energy distribution law of the normal spectrum. *Verhandl. Dtsch. phys. Ges.*, 2(237), 1900.

[3] P. A. M. Dirac. The Quantum Theory of the Emission and Absorption of Radiation. *Proceedings of the Royal Society A*, 114:243+, 1927.

[4] S. S. Schweber. *QED and the Men Who Made It: Dyson, Feynman, Schwinger and Tomonaga*. Princeton University Press, New Jersey, 1994.

[5] C. Cohen-Tannoudji, B. Diu, and F. Laloë. *Quantum Mechanics Vol. 1*. John Wiley & Sons, 1977.

[6] W. Gerlach and O. Stern. Das magnetische moment des silberatoms. *Zeitschrift für Physik*, 9(1):353–355, 1922. ISSN 0044-3328. doi: 10.1007/BF01326984. URL http://dx.doi.org/10.1007/BF01326984.

[7] D. P. DiVincenzo. Quantum computation. *Science*, 269:255, 1995.

[8] I. I. Rabi. On the process of space quantization. *Phys. Rev.*, 49:324–328, Feb 1936. doi: 10.1103/PhysRev.49.324. URL http://link.aps.org/doi/10.1103/PhysRev.49.324.

[9] D. Braak. Integrability of the rabi model. *Physical Review Letters*, 107(100401), Sept. 2011. URL http://link.aip.org/link/?RSI/69/1236/1.

[10] E. T. Jaynes and F. W. Cummings. Comparison of quantum and semiclassical radiation theories with application to the beam maser. *Proc. IEEE*, 51, 1963.

[11] H. J. Kimble. Strong interactions of single atoms and photons in cavity qed. *Physica Scripta*, 1998(T76):127, 1998. URL http://stacks.iop.org/1402-4896/1998/iT76/a=019.

[12] A. Wallraff, D.I. Schuster, Alexandre Blais, L. Frunzio, R.-S. Huang, J. Majer, S. Kumar, S.M. Girvin, and R.J. Schoelkopf. Strong coupling of a single photon to a superconducting qubit using circuit quantum electrodynamics. *Nature*, 431 (7005):162–167, 2004.

[13] I. Chiorescu, P. Bertet, K. Semba, Y. Nakamura, C. J. P. M. Harmans, and J. E. Mooij. Coherent dynamics of a flux qubit coupled to a harmonic oscillator. *Nature*, 431(7005):159–162, 2004. doi: 10.1038/nature02831. URL http://dx.doi.org/10.1038/nature02831.

[14] C. Ciuti, G. Bastard, and I. Carusotto. Quantum vacuum properties of the intersubband cavity polariton field. *Phys. Rev. B*, 72:115303, Sep 2005. doi: 10.1103/PhysRevB.72.115303. URL http://link.aps.org/doi/10.1103/PhysRevB.72.115303.

[15] C. Ciuti and I. Carusotto. Input-output theory of cavities in the ultrastrong coupling regime: The case of time-independent cavity parameters. *Phys. Rev. A*, 74:033811, Sep 2006. doi: 10.1103/PhysRevA.74.033811. URL http://link.aps.org/doi/10.1103/PhysRevA.74.033811.

[16] J. Casanova, G. Romero, I. Lizuain, J. J. García-Ripoll, and E. Solano. Deep strong coupling regime of the jaynes-cummings model. *Phys. Rev. Lett.*, 105:263603, Dec 2010. doi: 10.1103/PhysRevLett.105.263603. URL http://link.aps.org/doi/10.1103/PhysRevLett.105.263603.

[17] A. A. Anappara, S. De Liberato, A. Tredicucci, C. Ciuti, G. Biasiol, L. Sorba, and F. Beltram. Signatures of the ultrastrong light-matter coupling regime. *Phys. Rev. B*, 79:201303, May 2009. doi: 10.1103/PhysRevB.79.201303. URL http://link.aps.org/doi/10.1103/PhysRevB.79.201303.

[18] G. Scalari, C. Maissen, D. Turčinková, D. Hagenmüller, S. De Liberato, C. Ciuti, C. Reichl, D. Schuh, W. Wegscheider, M. Beck, and J. Faist. Ultrastrong coupling of the cyclotron transition of a 2d electron gas to a thz metamaterial. *Science*, 335(6074):1323–1326, 2012. doi: 10.1126/science.1216022. URL http://www.sciencemag.org/content/335/6074/1323.abstract.

[19] J. E. Mooij, T. P. Orlando, L. Levitov, Lin Tian, Caspar H. van der Wal, and Seth Lloyd. Josephson persistent-current qubit. *Science*, 285(5430):1036–1039, 1999. doi: 10.1126/science.285.5430.1036. URL http://www.sciencemag.org/content/285/5430/1036.abstract.

[20] T. P. Orlando, J. E. Mooij, Lin Tian, Caspar H. van der Wal, L. S. Levitov, Seth Lloyd, and J. J. Mazo. Superconducting persistent-current qubit. *Phys. Rev. B*,

60:15398–15413, Dec 1999. doi: 10.1103/PhysRevB.60.15398. URL http://link.aps.org/doi/10.1103/PhysRevB.60.15398.

[21] B. Peropadre, D. Zueco, D. Porras, and J. J. García-Ripoll. Nonequilibrium and nonperturbative dynamics of ultrastrong coupling in open lines. *Phys. Rev. Lett.*, 111:243602, Dec 2013. doi: 10.1103/PhysRevLett.111.243602. URL http://link.aps.org/doi/10.1103/PhysRevLett.111.243602.

[22] P. Forn-Díaz, J. Lisenfeld, D. Marcos, J. J. García-Ripoll, E. Solano, C. J. P. M. Harmans, and J. E. Mooij. Observation of the bloch-siegert shift in a qubit-oscillator system in the ultrastrong coupling regime. *Phys. Rev. Lett.*, 105:237001, Nov 2010. doi: 10.1103/PhysRevLett.105.237001. URL http://link.aps.org/doi/10.1103/PhysRevLett.105.237001.

[23] T. Niemczyk, F. Deppe, H. Huebl, E. P. Menzel, F. Hocke, M. J. Schwarz, J. J. Garcia-Ripoll, D. Zueco, T. Hümmer, E. Solano, A. Marx, and R. Gross. Circuit quantum electrodynamics in the ultrastrong-coupling regime. *Nature Physics*, 6 (10):772–776, 2010. doi: 10.1038/nphys1730. URL http://dx.doi.org/10.1038/nphys1730.

[24] A. Blais, R-S. Huang, A. Wallraff, S. M. Girvin, and R. J. Schoelkopf. Cavity quantum electrodynamics for superconducting electrical circuits: An architecture for quantum computation. *Phys. Rev. A*, 69:062320, Jun 2004. doi: 10.1103/PhysRevA.69.062320. URL http://link.aps.org/doi/10.1103/PhysRevA.69.062320.

[25] L. Mandel and E. Wolf. *Optical coherence and quantum optics*. Cambridge University Press, 1995.

[26] T. W. B. Kibble and F. H. Berkshire. *Classical Mechanics; 5th ed.* Imperial Coll., London, 2004.

[27] C. C. Gerry and P. L. Knight. *Introductory Quantum Optics*. Cambridge University Press, 2005.

[28] D. M. Pozar. *Microwave engineering; 3rd ed.* Wiley, Hoboken, NJ, 2005.

[29] P. Forn-Díaz. *Superconducting Qubits and Quantum Resonators*. Casimir PhD Series, TUDelft, 2010.

Index

Ceren Burçak Dağ was born in 1991 in Istanbul. She is an undergraduate student majoring in both Electronics and Telecommunications Engineering and Physics at Istanbul Technical University. She visited University of Waterloo (Canada) as an exchange student in 2014 and carried out her BSc research in Institute for Quantum Computing.